

# Co-opting the E3 ligase KLHDC2 for targeted protein degradation by small molecules

Received: 14 April 2023

Accepted: 4 October 2023

Published online: 04 January 2024

 Check for updates

Christopher M. Hickey<sup>1,4</sup>, Katherine M. Digianantonio<sup>1,4</sup>, Kurt Zimmermann<sup>1</sup> <sup>1</sup>, Alicia Harbin<sup>1</sup>, Connor Quinn<sup>1</sup>, Avani Patel<sup>1</sup>, Peter Gareiss<sup>1</sup> <sup>1</sup>, Amanda Chapman<sup>1</sup>, Bernadette Tiberi<sup>1,2</sup>, Jennifer Dobrodziej<sup>1,3</sup>, John Corradi<sup>1</sup>, Angela M. Cacace<sup>1</sup>, David R. Langley<sup>1</sup> & Miklós Békés<sup>1</sup> <sup>1</sup> 

Targeted protein degradation (TPD) by PROTAC (proteolysis-targeting chimera) and molecular glue small molecules is an emerging therapeutic strategy. To expand the roster of E3 ligases that can be utilized for TPD, we describe the discovery and biochemical characterization of small-molecule ligands targeting the E3 ligase KLHDC2. Furthermore, we functionalize these KLHDC2-targeting ligands into KLHDC2-based BET-family and AR PROTAC degraders and demonstrate KLHDC2-dependent target-protein degradation. Additionally, we offer insight into the assembly of the KLHDC2 E3 ligase complex. Using biochemical binding studies, X-ray crystallography and cryo-EM, we show that the KLHDC2 E3 ligase assembles into a dynamic tetramer held together via its own C terminus, and that this assembly can be modulated by substrate and ligand engagement.

The ubiquitin–proteasome system (UPS) is central to protein homeostasis in all eukaryotes, regulating numerous cellular processes and eliminating misfolded or damaged proteins<sup>1</sup>. Pharmacological hijacking of the UPS to eliminate disease-causing proteins has garnered considerable interest in recent years and is the centerpiece of a field known as targeted protein degradation (TPD)<sup>2</sup>. Ubiquitin is a small protein that can be covalently conjugated to other proteins in a process called ubiquitylation, which requires three enzymes in sequence: a ubiquitin-activating enzyme (E1), a ubiquitin-conjugating enzyme (E2), and a ubiquitin ligase (E3)<sup>3</sup>. TPD research has focused heavily on understanding and hijacking E3s, because they are the main substrate-recognizing component of the UPS. PROTACs are heterobifunctional small molecules comprising the ligand of an E3 ligase, a target-protein-binding ligand, and a linker connecting the two, affording induced proximity between the target and a ligase, resulting in the ubiquitylation and degradation of the target protein<sup>4</sup>. Although small molecule ligands exist for a few E3 ligases, most degrader compounds have been based on ligands for VHL and CRBN, substrate recognition subunits of specific E3 ligases in the Cullin-RING ligase family (CRLs), reviewed extensively in<sup>5</sup>. Only a few of the approximately 600 human E3 ligases have so far been applied in TPD<sup>6</sup>. Increasing the number of

E3s used in TPD will require the identification of ligands for additional E3 ligases. Exploring E3 ligases and their ligands beyond VHL and CRBN could provide more chemical choices for TPD applications.

CRLs encompass a subset of human E3 ligases and comprise about 250 combinations of substrate adapter proteins coupled to cullin scaffolds, and the substrate adapters have diverse structures and functions<sup>7</sup>. A subset of CRLs eliminate proteins with specific amino acid sequences in their carboxy termini<sup>8</sup>. Among these, three CRL2 substrate adapters—KLHDC2, KLHDC3, and KLHDC10—have been shown to control degradation of proteins that end with a glycine residue. In a study that measured the stability of thousands of green fluorescent protein (GFP)-tagged proteins bearing different C-terminal appendages, C termini ending in glycine were among the strongest at driving UPS-mediated degradation<sup>9</sup>. Transferable degradation-promoting sequences are called degrons, and those with critical C-terminal residues are called C-end degrons<sup>10</sup>. Of the three CRLs that recognize glycine-ending C-end degrons, CRL2<sup>KLHDC2</sup> has been studied in the greatest detail. The best substrates of CRL2<sup>KLHDC2</sup> end in a diglycine motif, which in some circumstances is generated by internal proteolytic cleavage of proteins<sup>8</sup>. High-resolution crystal structures of the substrate-binding kelch domain of KLHDC2 (KLHDC2<sub>KD</sub>) have been

<sup>1</sup>Arvinas, Inc, New Haven, CT, USA. <sup>2</sup>Present address: Genetics, Genomics and Cancer Biology Graduate Program, Thomas Jefferson University, Philadelphia, PA, USA. <sup>3</sup>Present address: Accent Therapeutics Inc, Lexington, MA, USA. <sup>4</sup>These authors contributed equally: Christopher M. Hickey, Katherine M. Digianantonio. ✉e-mail: [miklos.bekes@arvinas.com](mailto:miklos.bekes@arvinas.com)

determined in the presence of diglycine-ending substrate peptides, offering atomic-level detail of C-end degron recognition<sup>11</sup>. Thus, CRL2<sup>KLHDC2</sup> is an E3 ligase that can drive rapid degradation of its substrate proteins and that has a well-characterized substrate-recognition pocket, making it an attractive potential option for TPD<sup>12–14</sup>. However, to our knowledge, no small molecules have been developed that target KLHDC2, so it has thus far not been possible to investigate whether KLHDC2 could be co-opted for TPD using heterobifunctional PROTAC degrader molecules.

To discover additional E3 ligases for TPD, we sought to functionalize KLHDC2 as a PROTAC-employable E3 ligase using small molecules. Herein we describe the discovery and biochemical and structural characterization of small-molecule ligands targeting KLHDC2. We functionalize these novel KLHDC2-targeting small molecules into robust and potent KLHDC2-based BET-family and AR protein PROTAC degraders and demonstrate that such degradation is KLHDC2-dependent. Finally, we offer insight into the assembly of the KLHDC2 holo-E3 complex together with its cognate adapter proteins, EloB and EloC. We show, using biochemical binding studies, X-ray crystallography, and cryogenic electron microscopy (cryo-EM), that the KLHDC2 E3 ligase assembles into a dynamic tetramer, which is held together via its C termini, and that this assembly can be modulated by both substrate and small-molecule engagement. Altogether, this work expands the arsenal of E3 ligases that can be targeted by small molecules and can be hijacked for PROTAC-induced targeted protein degradation.

## Results

### Discovery of KLHDC2-targeting small molecules

To identify small molecules that can bind KLHDC2, we used computational de novo small-molecule discovery and tested whether these small molecules could interact with KLHDC2. Using computer-aided drug design (CADD), we started with the available crystal structure of KLHDC2<sub>KD</sub> bound to its cognate C-terminal substrate degron, SelK, anchored by its C-terminal glycine residue (Protein Data Bank (PDB) 6DO3 ref. 11). The terminal glycine (Gly91) of the SelK peptide—which binds most deeply into the substrate pocket and makes four hydrogen bonds (H-bonds, yellow dotted lines) with Ser269, Arg241, and Arg236—was retained, whereas Gly90 was replaced with a pyridinone ring (Fig. 1a, step 1). The pyridinone ring forms  $\pi$ -cation bonds with Arg236 and Lys147 from its top and bottom face and mimics the carbonyl group of Gly90 to form an H-bond with Trp191 (Fig. 1a, step 1). A naphthyridinone ring was added that forms an H-bond with Lys147 to reinforce the  $\pi$ -cation interactions with the pyridinone ring (Fig. 1a, step 2). The bulky naphthyridinone ring enforces a non-planar conformation between the two ring systems, guiding the sec-butyl or isobutyl group of KDRLKZ-1 and KDRLKZ-2, respectively, both of which mimic Pro87 of the SelK peptide, into a hydrophobic pocket composed of Tyr50, Leu342, Leu343, Trp321, and Trp370 (Fig. 1a, step 3) while placing the linker carbamate near Arg236 for transient H-bonding and directing the linker out of the pocket toward the zone of ubiquitination<sup>2</sup> (Fig. 1a, step 4). We relied on cycles of de novo design and compound synthesis to further optimize these new small molecules, and continuous iterative cycles of direct binding experiments using surface plasmon resonance (SPR) to generate data to inform ligand optimization. Compounds were also assayed for their ability to displace a SelK peptide as measured by an alphaLISA displacement assay. This ultimately led to the discovery of a series of small-molecule ligands that potently engaged KLHDC2<sub>KD</sub> (Fig. 1a–i).

To assess the specificity of both the KLHDC2 assay and the newly identified KLHDC2 small-molecule ligands (Fig. 1b), we compared a VHL-targeting small molecule, VH298 (ref. 15), with the KLHDC2 ligands in a KLHDC2<sub>KD</sub> alphaLISA assay (Fig. 1c), and in a VHL alphaLISA assay (Fig. 1d). KDRLKZ-1, as a representative small molecule in the lead series, has shown ligand displacement in the KLHDC2<sub>KD</sub> alphaLISA, but

not in the VHL alphaLISA, and vice versa for VH298 (Fig. 1c,d). Direct binding of KDRLKZ-1 to KLHDC2<sub>KD</sub> was also tested by SPR, displaying a 1:1 binding mode (Fig. 1e). Biochemical and biophysical binding constants for KDRLKZ-1, KDRLKZ-2, and KDRLKZ-3 are shown in a table (Fig. 1f). KDRLKZ-1 was shown to bind KLHDC2<sub>KD</sub> with a  $K_d$  of 0.36  $\mu$ M by SPR, produced a +6.8 °C shift by thermal-shift assay, and displaced the SelK peptide with a half-maximal inhibitory concentration ( $IC_{50}$ ) of 0.21  $\mu$ M and 0.31  $\mu$ M as measured by alphaLISA and time-resolved fluorescence resonance energy transfer (TR-FRET) displacement assays, respectively. Replacing the acid moiety of KDRLKZ-1 with an amide functionality resulted in reduced binding, consistent with the binding mode of C-terminal peptides to KLHDC2 (refs. 9,11). Compounds in which the acid moiety has been replaced with an amide will be referred to as ‘E3 dead’ compounds (such as KDRLKZ-3, shown in Fig. 1b), which no longer bind to KLHDC2.

The binding pose of KDRLKZ-1 in the substrate-binding pocket of KLHDC2<sub>KD</sub> was confirmed by a co-crystal structure (Fig. 1g–i and Table 1). As shown, KDRLKZ-1 fills the KLHDC2 substrate-binding pocket and makes interactions analogous to those of natural substrates, with the C-terminal acid anchor shown to overlay with the C terminus of SelK (Fig. 1h). As predicted by our original de novo CADD model for KDRLKZ-1, the carboxylic acid makes four H-bonds or salt bridge interactions with KLHDC2; the pyridinone forms an H-bond with Trp191 and makes  $\pi$ -cation interactions with Arg236 and Lys147 from the top and bottom faces; the naphthyridinone ring sterically enforces a non-planar conformation, guiding the carbonyl to form an H-bond with Lys147 and placing the sec-butyl group into a hydrophobic pocket; and the linker carbamate sits near Arg236 and points out of the pocket (Fig. 1i).

To further characterize KLHDC2 ligands, we purified full-length KLHDC2 E3 ligase in complex with its cognate adapters, EloB and EloC (the complex is hereafter referred to as KBC) and conducted ubiquitylation experiments with the native substrate, a USP1-peptide labeled with a cyanine 5 fluorophore. We used fluorescence to monitor ubiquitin-chain formation on USP1 in a gel-based readout in the absence or presence of KLHDC2-targeting small molecules. First, we determined that USP1 ubiquitylation was KLHDC2-dependent (Extended Data Fig. 1a). Then, we showed that excess substrate, as well as the small-molecule ligand KDRLKZ-1, can compete with USP1 for ubiquitylation by KLHDC2 (Extended Data Fig. 1b). These experiments demonstrated that the purified KBC was active and that it could be engaged by KLHDC2-targeting small molecules.

Altogether, we show that KLHDC2-targeting small molecules, such as KDRLKZ-1, bind to KLHDC2 in its substrate-binding pocket and can displace its natural substrate.

### KLHDC2 small molecules can function in induced proximity

To test the ability of the new KLHDC2 ligands to engage KLHDC2 when incorporated into heterobifunctional molecules, we tested whether one such KLHDC2 ligand could retrieve KLHDC2 from cell extracts using an assay that has previously been used to investigate multiple E3 ligases and their small-molecule ligand-derived chemical probes<sup>16</sup>. To this end, a biotin-conjugated KLHDC2 ligand was designed and generated (Extended Data Fig. 1c) and was subsequently used to create streptavidin–agarose affinity beads. To analyze cellular engagement and the interaction with KLHDC2, cells were transiently transfected with HiBiT-KLHDC2. KLHDC2 pull-down, facilitated by the interaction with the immobilized ligand on agarose beads, was quantified using the HiBiT signal. A similar assay was developed for VHL to measure the interaction with its ligand. For both VHL and KLHDC2, the HiBiT signal was substantially higher for beads bearing the specific probe targeting the respective ligase than for beads conjugated with biotin alone (Fig. 2a). Furthermore, the biotin-labeled KLHDC2-ligand probe could bind endogenous KLHDC2 from cell extracts (Fig. 2b), and this interaction could be competitively inhibited by excess ligand

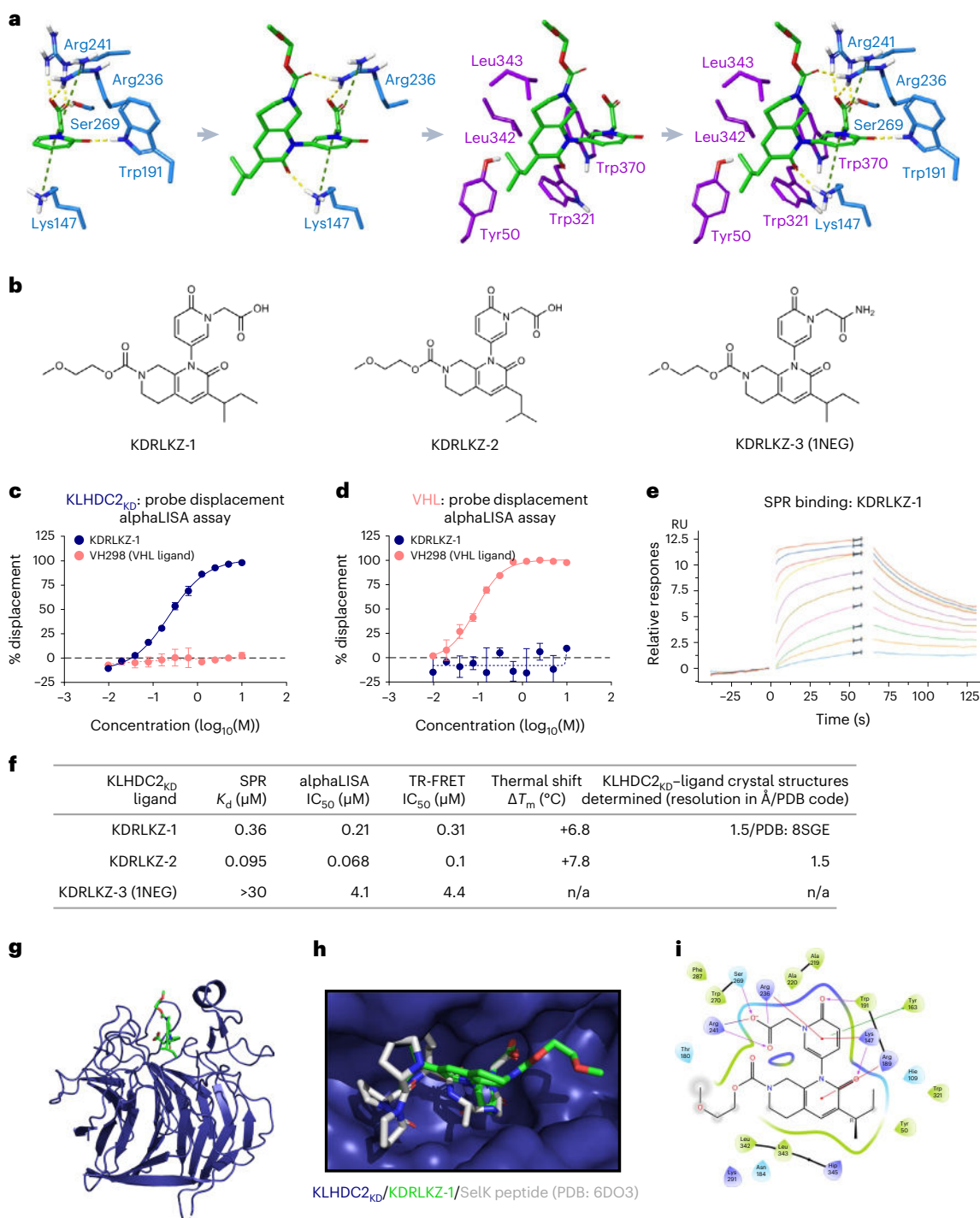


**Fig. 1 | Discovery of high-affinity small-molecule ligands, by structure-based de novo design, targeting the substrate-binding kelch domain of KLHDC2.**

**a**, Schematic view of the CADD-based de novo ligand-discovery workflow to identify KLHDC2 ligands (see text for details). **b**, Structures of (representative) KLHDC2 small-molecule ligands (1NEG refers to an E3-dead version of KDRLKZ-1, see text for details). **c, d**, Activities of KDRLKZ-1 and a VHL ligand in a KLHDC2-targeting alphaLISA displacement assay (**c**), and in a VHL-targeting alphaLISA displacement assay (**d**), showing the specificity of each small molecule for their respective displacement assay. KDRLKZ-1 is shown in blue, and VHL298 is shown in pink (the alphaLISA experiments have a minimum of 5 biological replicates, one  $n = 2$  replicate set is shown; data are shown as mean  $\pm$  s.d.). **e**, SPR binding

sensograms of KDRLKZ-1 against KLHDC2 ( $n = 10$  biological replicates, one set shown).  $T_m$ , melting temperature. **f**, Biochemical and biophysical characteristics of KLHDC2 ligands (data are shown as geometric means). **g**, Overall view of the co-crystal structures of KDRLKZ-1 bound to KLHDC2<sub>KD</sub> in ribbon representation (KLHDC2<sub>KD</sub> in blue, KDRLKZ-1 in green, PDB 8SGE). **h**, Overlay of the binding pose of KDRLKZ-1 and a KLHDC2 substrate, with the C terminus of SelK (PDB 6D03) in the substrate-binding pocket. **i**, Two-dimensional protein-ligand interaction map of from the crystal structure of KDRLKZ-1 bound in the substrate-binding pocket of KLHDC2<sub>KD</sub> (PDB 8SGE, see text for details). Hip and Hie refer to different protonation states of the amino acid His). Map was generated by Maestro (Schrodinger).

**Table 1 | Data collection and refinements statistics for the two X-ray structures presented**

	KLHDC2 <sub>KD</sub> -KDRLKZ-1 (8SGE)	KLHDC2 <sub>KD</sub> -C-term1 (8SGF)
Data collection <sup>a</sup>		
Space group	<i>P</i> <sub>2</sub> <sub>1</sub>	<i>P</i> <sub>2</sub> <sub>1</sub>
Cell dimensions		
<i>a</i> , <i>b</i> , <i>c</i> (Å)	44.90, 88.49, 89.22	44.51, 88.19, 89.34
$\alpha$ , $\beta$ , $\gamma$ (°)	90.000, 104.449, 90.000	90.00, 104.49, 90.00
Resolution (Å)	86.398–1.509 (1.611–1.509)	19.798–1.418 (1.552–1.418)
<i>R</i> <sub>merge</sub>	0.064 (0.869)	0.062 (0.747)
<i>I</i> / $\sigma$ ( <i>I</i> )	9.4 (1.4)	10.4 (1.5)
Completeness (%)	76.9 (21.7)	68.7 (14.6)
Redundancy	81,396 (4,071)	86,639 (4,332)
Refinement		
Resolution (Å)	86.40–1.509 (1.57–1.51)	86.40–1.42 (1.51–1.42)
No. reflections	81,396 (1,628)	86,639 (1,733)
<i>R</i> <sub>work</sub> / <i>R</i> <sub>free</sub>	0.1787 (0.2241) / 0.2065 (0.2237)	0.1992 (0.2126) / 0.2280 (0.2589)
No. atoms	5,989	5,987
Protein	5,246	5,363
Ligand/ion	120	30
Water	623	594
<i>B</i> factors		
Protein	31.05	28.99
Ligand/ion	29.46	27.90
Water	38.48	33.14
R.m.s. deviations		
Bond lengths (Å)	0.008	0.008
Bond angles (°)	0.95	0.96

<sup>a</sup>Values in parentheses are for the highest-resolution shell.

(Extended Data Fig. 1d). Encouraged by the engagement of KLHDC2 by a biotin-functionalized, heterobifunctional molecule, we conducted orthogonal experiments to induce proximity between KLHDC2 and target proteins.

Using JQ1 as a target binding ligand<sup>17</sup>, we generated a series of KLHDC2–BRD4 PROTAC molecules (Fig. 2c–e) using active and E3-dead versions of the KLHDC2 ligands (Fig. 2c) and tested their ability to form ternary complexes, as measured by SPR (Fig. 2d,e). In our ternary-complex SPR experiments, we immobilized a His-tagged bromodomain from BRD4 on an SPR chip and presented the KLHDC2–BRD4 PROTAC molecules in the absence or presence of GST-tagged KLHDC2<sub>KD</sub>. One PROTAC molecule, K2-B4-3, exhibited strong ternary-complex formation (Fig. 2d). The efficiency of ternary-complex formation was dependent on KLHDC2 recruitment, as the E3-dead version, K2-B4-3d, did not form a ternary complex. Ternary-complex formation was also dependent on linker length and composition: a longer, structured linker was necessary for optimal efficiency (Fig. 2e and Extended Data Fig. 1e). For all tested PROTAC molecules, the formation of ternary complexes did not involve cooperative interactions.

Taken together, our results demonstrate that KLHDC2-based molecules can function in a heterobifunctional manner to induce proximity.

## Degradation of BET-family and AR proteins by KLHDC2-based PROTAC degraders

Having created PROTACs that can induce ternary-complex formation between BRD4<sub>BD2</sub> and KLHDC2<sub>KD</sub>, we next tested whether these PROTACs could drive effective degradation of BRD4 in cells. We began with CRISPR-edited cells in which an amino-terminal HiBiT tag had been added to endogenous BRD4 for quantitative and high-throughput measurements of BRD4 levels<sup>18</sup>. KLHDC2–BRD4 PROTAC molecules were generated with one of two linker types and one of three types of KLHDC2 ligand: carboxylic acid, methyl ester, or amide (Fig. 3a). The selected methyl ester group acts as a prodrug, converting into a carboxylic acid after cell entry and processing by cellular esterases<sup>19</sup>. We used this strategy because compounds with acid groups have sub-optimal cellular permeability. The amide-based PROTAC molecules were designed to serve as E3-dead negative controls (Figs. 1 and 2). The KLHDC2–BRD4 PROTAC molecules containing the methyl ester KLHDC2 ligand were fast and efficient at degrading HiBiT–BRD4, with a 93% reduction within 4–6 h (Fig. 3b,c). Heterobifunctional PROTAC degraders with the acid group also degraded HiBiT–BRD4, but less so than the ester-containing molecules (degradation kinetics at 6 h are shown as a table in Figure 3d). In accordance with SPR data (Fig. 2), structured linkers were more efficient at degrading BRD4. As expected, PROTAC molecules with the amide group showed little to no activity in the HiBiT–BRD4 assay (Fig. 3d and Extended Data Fig. 2a).

To determine whether KLHDC2–BRD4 PROTAC molecules can induce degradation of endogenous BRD4, we performed immunoblots for BRD4 in several cell lines after treatment with the KLHDC2-directed PROTAC molecules. Interestingly, although PROTAC molecules such as K2-B4-3e induced BRD4 degradation in most cell lines, the extent of that degradation varied (Extended Data Fig. 2b and unpublished data). By contrast, a control CRBN–BRD4 PROTAC<sup>20</sup> was comparably active in all tested cell lines. To confirm that the observed BRD4 degradation was dependent on the UPS, we assessed HiBiT–BRD4 levels in the presence or absence of the proteasome inhibitor MG-132 or the neddylation inhibitor MLN-4924. Both of these UPS inhibitors prevented the loss of luminescence that was otherwise observed in the presence of K2-B4-5e (Fig. 3e). Similar data were obtained for K2-B4-3e when assessed using the HiBiT assay or immunoblot (Extended Data Fig. 2c). Furthermore, in mouse A20 cells, BRD4 degradation was observed with K2-B4-5 and K2-B4-5e, but not with K2-B4-5d (Extended Data Fig. 2d). These results demonstrate that BRD4 degradation was nearly equivalent across species, in line with the high amino acid sequence conservation (97%) of KLHDC2 proteins between mice and humans.

To test whether the activity of our KLHDC2–BRD4 PROTAC molecules was dependent on KLHDC2, we used small interfering RNA (siRNA) to knock down genes. Knocking down *KLHDC2* completely blocked HiBiT–BRD4 degradation induced by K2-B4-5e (Fig. 3f and Extended Data Fig. 2e). As a control, siRNA-mediated knockdown of an unrelated E3 ligase, DCAF16, had no effect on KLHDC2-mediated BRD4 degradation (Fig. 3f). As a control for DCAF16, treatment with a *DCAF16*-targeting siRNA did reduce the activity of compound 1 (originally designed as a DCAF15-based BRD4-targeting PROTAC from a patent)<sup>21</sup>, which degrades BRD4 and is unrelated to KLHDC2 (Extended Data Fig. 3a). We chose DCAF16 as a control because, in tandem with our work on KLHDC2, we determined that the activity of compound 1 was instead dependent on DCAF16 (Extended Data Fig. 3a–d). Interestingly, two recent publications have reported similar findings and provide mechanistic and structural details of DCAF16-mediated degradation of BRD4 induced by BRD4-targeting monovalent compounds<sup>22</sup> and by compound 1 (ref. 23). We also confirmed knockdown of KLHDC2 by the siRNAs using two methods: quantitative PCR (qPCR) (Extended Data Fig. 2f), and stabilization of a model diglycine degron-containing substrate of CRL2<sup>KLHDC2</sup> (Extended Data Fig. 4a–d,e). Akin to GFP-degron proteins<sup>9</sup>, we created constructs and corresponding cell lines expressing nanoluc-degron (NLD) proteins,

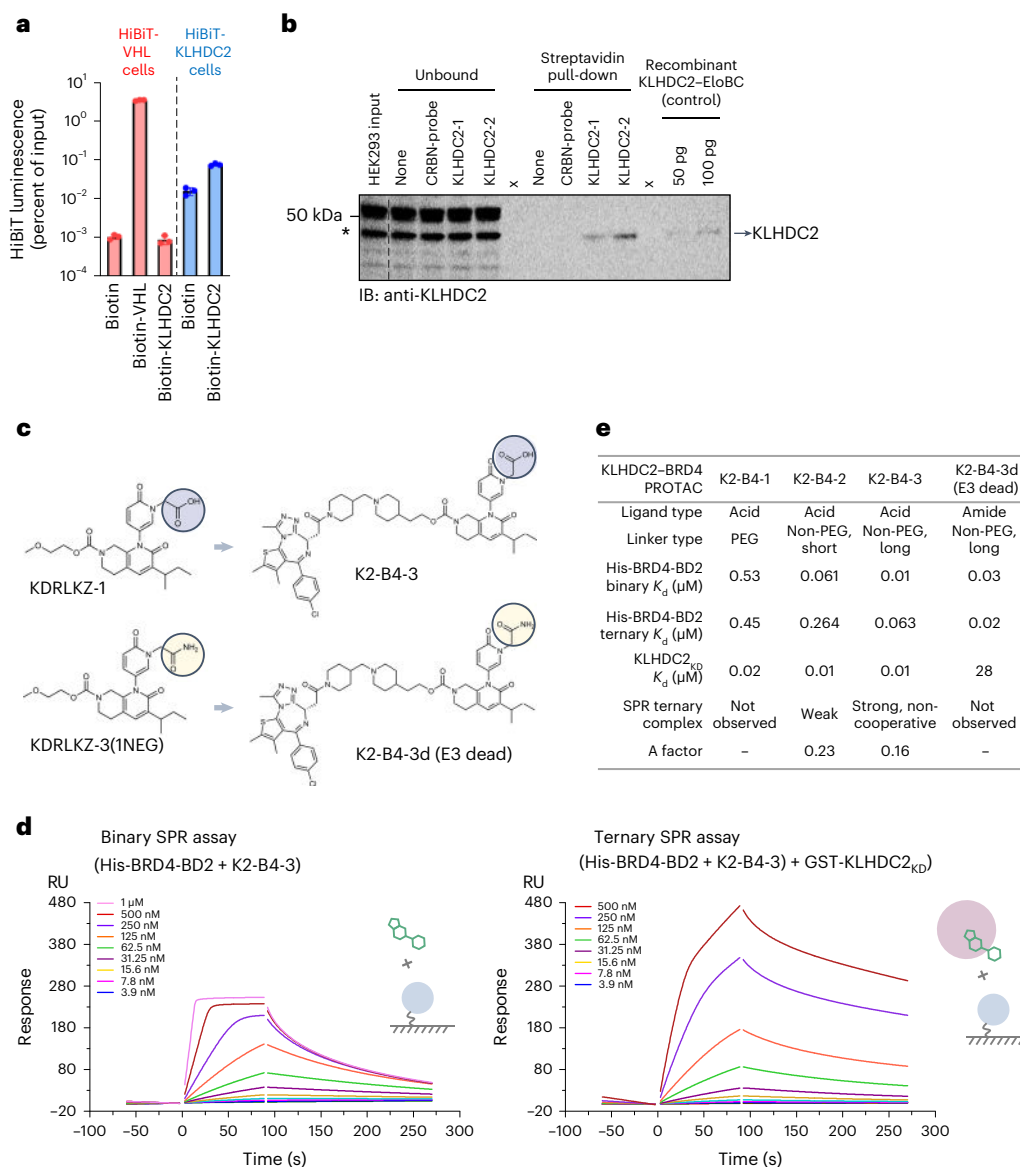


**Fig. 2 | Functionalized KLHC2-targeting small molecules, when incorporated into heterobifunctional molecules, bring KLHC2 and target proteins into closer proximity. a**, Streptavidin bead pull-down assay of HiBiT-KLHC2 and HiBiT-VHL from cell lysates, analyzed by HiBiT luminescence ( $n = 3$  technical replicates shown). **b**, Streptavidin bead pull-down assay of endogenous KLHC2 from cell lysates, analyzed by immunoblot (IB) using an anti-KLHC2 antibody. KLHC2-1 and KLHC2-2 indicate replicate affinity beads bearing the biotin-conjugated KLHC2 ligand. \*In KLHC2 immunoblots, a band present in cell extracts that migrated as an approximately 46-kDa species is not KLHC2.

See the Methods section for more information. **c**, Structures of active (acid, blue) and inactive (amide, yellow) KLHC2 ligands and their corresponding JQ1-based KLHC2-BRD4 PROTAC molecules. **d**, Binary and ternary SPR sensograms of a KLHC2-BRD4 PROTAC (green schematic) binding immobilized His-tagged BRD4-BD2 (blue circle on chip surface) in the absence or presence of GST-tagged KLHC2<sub>KD</sub> (pink circle). **e**, Biophysical binding characteristics of KLHC2-BRD4 PROTAC molecules as measured by ternary complex SPR experiments (more SPR binding sensograms are shown in Extended Data Fig. 1b).

whose abundance could be measured by luminescence (Extended Data Fig. 4a). An NLD fused with a diglycine degenon specific to KLHC2 was stabilized by MLN-4924 treatment (Extended Data Fig. 4b). Using these NLD cells, we showed that treatment with three separate siRNAs targeting *KLHC2* led to increases of more than tenfold in the levels of this NLD protein (Extended Data Fig. 4c). Consistent with published data, the expression levels of a similar NLD containing a KLHC3 degenon were affected by knockdown of KLHC3, but not of KLHC2 (Extended Data Fig. 4d).

In our studies, we observed BRD2 and BRD3 degradation across cell lines with our KLHC2-BRD4 PROTAC molecules (Fig. 3g). This outcome was not unexpected, as other PROTACs based on CRBN or VHL, with JQ1 as a target warhead, exhibit these properties<sup>18</sup>. As is the

case for BRD4, BRD2 degradation by K2-B4-5e was completely blocked by KLHC2 knockdown (Fig. 3g), but not by DCAF16 knockdown.

To expand the scope of proteins that can be targeted for degradation by KLHC2-based PROTAC degraders, we generated androgen receptor (AR)-targeting KLHC2-based PROTAC degraders, such as K2-AR-1 (Fig. 3h). Similar to BET-family proteins, AR was degraded by a KLHC2-based PROTAC in a UPS-dependent manner (Fig. 3i); AR degradation by K2-AR-1 was also shown to be dependent on KLHC2 (Fig. 3j).

Taken together, our cellular KLHC2-based BRD4 and AR degradation data show that our PROTAC molecules, such as K2-B4-5e and K2-AR-1, are capable of inducing rapid and robust degradation of BET-family and AR proteins in cells, and that such degradation is dependent on the UPS and KLHC2.

### Purified full-length KLHDC2–EloB–EloC E3 ligase complex is a dynamic oligomer

During purification of the full-length KBC E3 ligase (KLHDC2 in complex with EloB and EloC) used in the functional *in vitro* ubiquitylation experiments to assess its activity, we observed that KBC eluted from the size-exclusion chromatography columns at a size larger than its predicted molecular weight. Indeed, analytical size-exclusion chromatography of the KBC complex showed one predominant peak with an elution profile consistent with a complex with a molecular weight of approximately 200 kDa (Fig. 4a, gray trace, and Fig. 4b, top gel). Although co-purification of substrates has been seen in some recombinant preparations of substrate adapters<sup>24,25</sup>, SDS–PAGE and liquid chromatography–tandem mass spectrometry (LC–MS) analysis showed no signs of contamination in the KBC complex. High-mass, intact matrix-assisted laser desorption/ionization (MALDI) analysis revealed that a mixture of species, consisting of one to four KBC complexes, was present in the sample (Extended Data Fig. 5a, blue trace).

Strikingly, the elution profile of KBC shifted upon incubation with its substrate, a SelK peptide. This shift, observed during analytical size-exclusion chromatography experiments, was found to be concentration-dependent, with SelK causing a rightward shift in the elution of KBC. The right-shifted elution profile of the KBC–SelK peptide complex matched the expected molecular weight, consistent with one KBC complex (Fig. 4a, blue traces, and Fig. 4b, bottom gel). We observed a shift in the mass profile of the KBC–SelK peptide complex in intact-mass MALDI experiments as well (Extended Data Fig. 5a, red trace).

These observations led us to hypothesize that the KBC complex is a dynamic oligomer that can be influenced by substrate binding into its KLHDC2<sub>kd</sub> pocket. Because KLHDC2 is an E3 ligase that recognizes C-terminal GlyGly-ending peptides as substrates, we wondered whether its own C terminus (which terminates in GlySer) could be involved in this dynamic complex formation. Indeed, short peptides derived from the C terminus of KLHDC2 could displace the substrate SelK in an alphaLISA displacement assay (Fig. 4c), albeit with low affinity (Fig. 4d). Consistent with their weaker binding affinity, incubating these peptides with KBC *in trans* resulted in partial dissociation of a KBC oligomer (Fig. 4e and Extended Data Fig. 5b).

Next, we sought to understand the structure of KLHDC2<sub>kd</sub> in complex with its C-terminal peptide *in trans*. A co-crystal structure of a KLHDC2 C-terminal peptide in complex with KLHDC2<sub>kd</sub> revealed that its binding pose was identical to that of one of its natural substrates, SelK (Fig. 4f and Table 1). As shown, there was a slight shift of Trp270 to accommodate the extra atoms of Ser406, but otherwise, key interactions with Arg236 were preserved.

Altogether, our biochemical characterizations of KBC complex dynamics suggest that KLHDC2 exists in a higher order oligomeric state that can be modulated via occupancy of its substrate-binding pocket, perhaps by its own C terminus.

### Cryo-EM reveals that the KLHDC2–EloB–EloC complex is a tetramer

To define the nature of the oligomeric KBC species in more detail, we performed single-particle cryo-EM on a chemically cross-linked KBC complex (Extended Data Fig. 6a). Single-particle analysis (Extended

Data Fig. 6b–e) of the KBC complex and initial model generation in cryoSPARC<sup>26</sup> revealed a heterogeneous population of KBC complexes, but most particles were KBC tetramers. Three-dimensional (3D) variability analysis in cryoSPARC of the tetrameric complex yielded classes that differed in the density of the four EloBC subunits. Further refinement of a small set of particles with the most complete density suggested a symmetric arrangement of the KBC molecules as a dimer of dimers.

Therefore, we applied C<sub>2</sub> symmetry in a non-uniform refinement<sup>27</sup> to obtain the 3D reconstruction of the full-length KBC complex at a final resolution of 3.8 Å (Fig. 5a and Table 2). One half of the symmetric complex consists of two KBC subcomplexes; we colored one protomer purple and named it KLHDC2<sub>1</sub>, and we colored the other orange and named it KLHDC2<sub>2</sub>. In each subcomplex, KLHDC2 is saturated, while the respective EloB and EloC binding partners are colored in lighter shades (Fig. 5a).

The kelch domains of KLHDC2, EloB, and EloC were unambiguously modeled in the map, and there was additional density at the interface of consecutive kelch domains, where they interacted with EloB and EloC. An overlay of non-symmetric KBC units shows that the BC-box binding of KLHDC2 to EloB and EloC is mediated by Leu364, Ser366, and Val372 of KLHDC2 (Extended Data Fig. 7a). Although the BC boxes overlap, the remaining parts of the C terminus of KLHDC2 do not. The remainder of the C terminus corresponds to the predicted Cullin box of KLHDC2 (ref. 28). As shown in Extended Data Figure 7b, only the purple KLHDC2<sub>1</sub> Cullin boxes are properly positioned to interact with CUL2 in the tetramer, whereas the KLHDC2<sub>2</sub> Cullin box is not. Using analytical size-exclusion chromatography, we show that CUL2 can form a complex with KBC (Extended Data Fig. 7c).

Our model further demonstrates that the interactions between consecutive KLHDC2 molecules are mediated by the ends of the N and C termini of KLHDC2<sub>1</sub>. First, one set of interactions is mediated by residues 400–406 of KLHDC2<sub>1</sub> binding to the substrate-binding site of KLHDC2<sub>2</sub> (Fig. 5b). These interactions closely resemble those observed in the crystal structure described above with its C-terminal peptide. Second, C-terminal residues of KLHDC2<sub>1</sub> in the BC and Cullin boxes also interact with KLHDC2<sub>2</sub> (Fig. 5b, inset). Lys376 of KLHDC2<sub>1</sub> forms an H-bond with Asn184 in the backbone of KLHDC2<sub>2</sub>; Glu377 of KLHDC2<sub>1</sub> forms an H-bond with His345 of KLHDC2<sub>2</sub>; and Phe375 of KLHDC2<sub>1</sub> forms hydrophobic interactions with Leu58 of KLHDC2<sub>2</sub>. Third, we observe N-terminal residues of KLHDC2<sub>1</sub> extending toward KLHDC2<sub>2</sub>, although it is difficult to explain specific interactions at this resolution. We do not see any specific interactions between this face of the kelch domains of KLHDC2<sub>1</sub> and KLHDC2<sub>2</sub>.

Continuing along the daisy chain of KBC protomers, numerous interactions between KLHDC2<sub>2</sub> and KLHDC2<sub>1</sub>' are apparent. The C terminus of KLHDC2<sub>2</sub> is rearranged to 'open up' of the BC and Cullin boxes, which lasso around EloC<sub>2</sub> and bring KLHDC2<sub>1</sub> and EloC<sub>2</sub> into close proximity (Fig. 5c). Residues 363–397 of KLHDC2<sub>2</sub>, which form this lasso, have been roughly modeled in our map (Fig. 5c, inset). The resolution is not sufficient to conclusively describe most interactions in this region. However, it is clear that, at the end of this lasso, residues 400–406 of KLHDC2<sub>2</sub> bind into the substrate-binding pocket of KLHDC2<sub>1</sub>'. There are also significant interactions between the Kelch domains of KLHDC2<sub>2</sub> and KLHDC2<sub>1</sub>' on this face. One patch is mediated by Glu179, Thr180,

**Fig. 3 | Degradation of BET-family proteins and AR by KLHDC2-based PROTACs.** **a**, Structures of methyl-ester-containing KLHDC2–BRD4 PROTAC molecules. **b**, HiBiT–BRD4 degradation curves of the KLHDC2–BRD4 PROTACs shown in **a**. **c**, Time course of HiBiT–BRD4 degradation by the K2–B4–5e PROTAC at 2, 4 and 6 h ( $n = 2$ ). DC<sub>50</sub>, the PROTAC concentration that produces half-maximal degradation;  $D_{max}$ , the maximal extent of degradation. **d**, Degradation parameters of certain KLHDC2–BRD4 PROTAC degraders in PC-3 cells at 6 h against HiBiT–BRD4 ( $n = 2$  minimum, geometric means shown). ND, no data. **e**, HiBiT–BRD4 degradation curves of the K2–B4–5e PROTAC in the presence of the UPS inhibitors MG-132 and MLN-4924 ( $n = 2$ ,  $n = 1$  for MG-132). **f**, HiBiT–BRD4

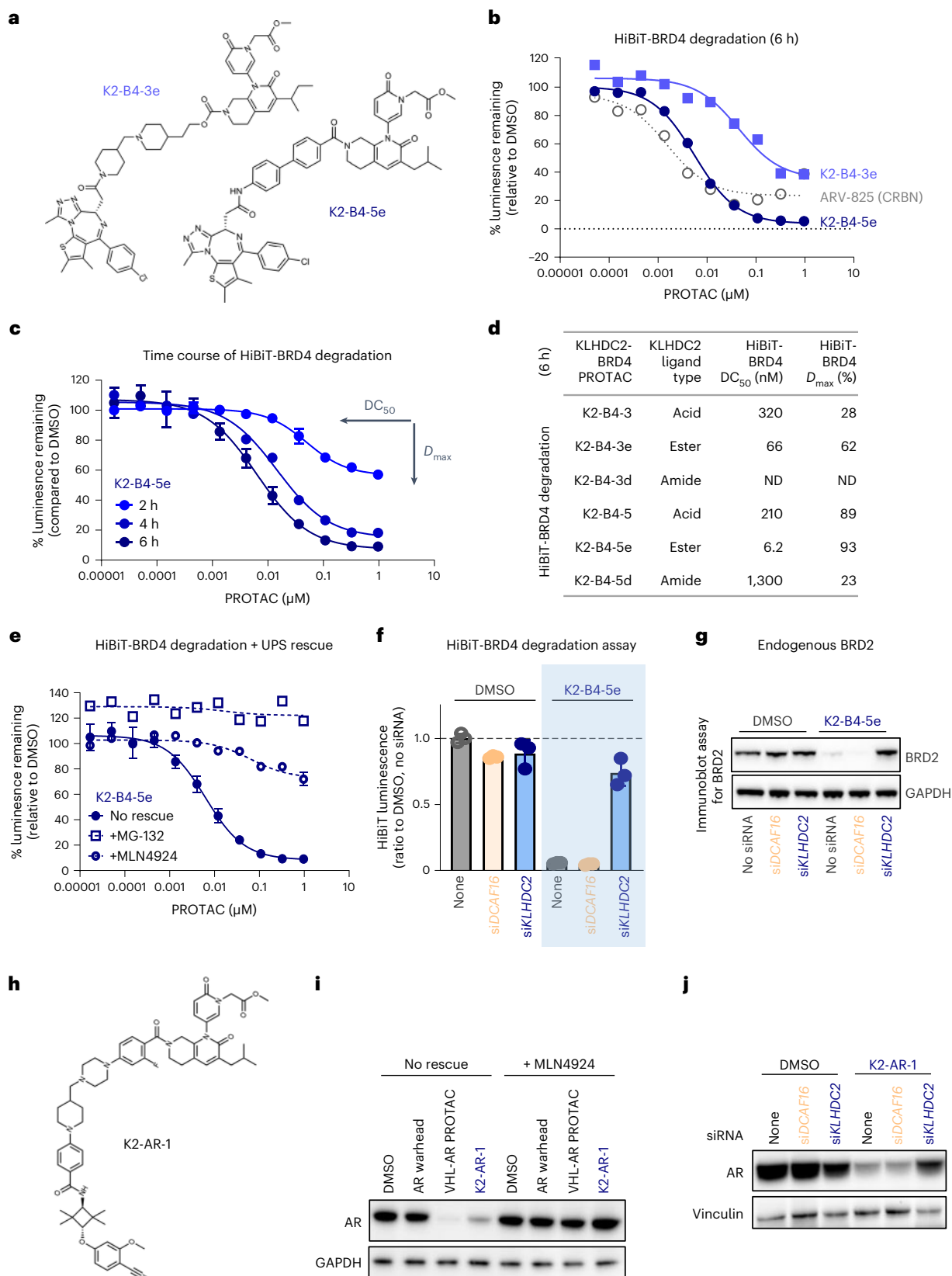
luminescence values of cells that were treated with the indicated siRNAs for 48 h, and then were treated with the K2–B4–5e PROTAC ( $n = 3$ ). **g**, BRD2 immunoblot of cells treated with the indicated siRNAs for 48 h, then with the K2–B4–5e PROTAC. The samples were the same as those analyzed in **f**. **h**, Structures of the KLHDC2–AR PROTAC. **i**, AR immunoblot of cells treated with PROTAC degraders for 12 h in the absence or presence of MLN-4924 (1 μM). **j**, AR immunoblot of cells that were treated with the indicated siRNAs for 72 h, and then with the K2–AR-1 PROTAC for 12 h. **g–j**, BRD and AR degradation were rescued by siKLHDC2, but not by siDCAF16. Immunoblots represent at least two biological replicates. Data are shown as mean ± s.d.

and Trp183 of KLHDC2<sub>1</sub>' and residues 74–77 of KLHDC2<sub>2</sub>. A second patch is mediated by His346 and Arg347 of KLHDC2<sub>1</sub>' and Asp127 of KLHDC2<sub>2</sub> (Fig. 5c, inset).

Thus, our cryo-EM model and our biochemical data suggest that KLHDC2 tetramers are held together by a low-affinity interaction mediated by the C termini of KLHDC2 proteins binding to adjacent

substrate-binding pockets. Higher affinity substrates are thought to displace KLHDC2 C termini and thus to break up the oligomers into smaller dimeric and monomeric species.

Consistent with their attributes as high-affinity KLHDC2 ligands, our series of KLHDC2-targeting small molecules are also able to modulate KBC tetramer dynamics (some better than others), as shown by



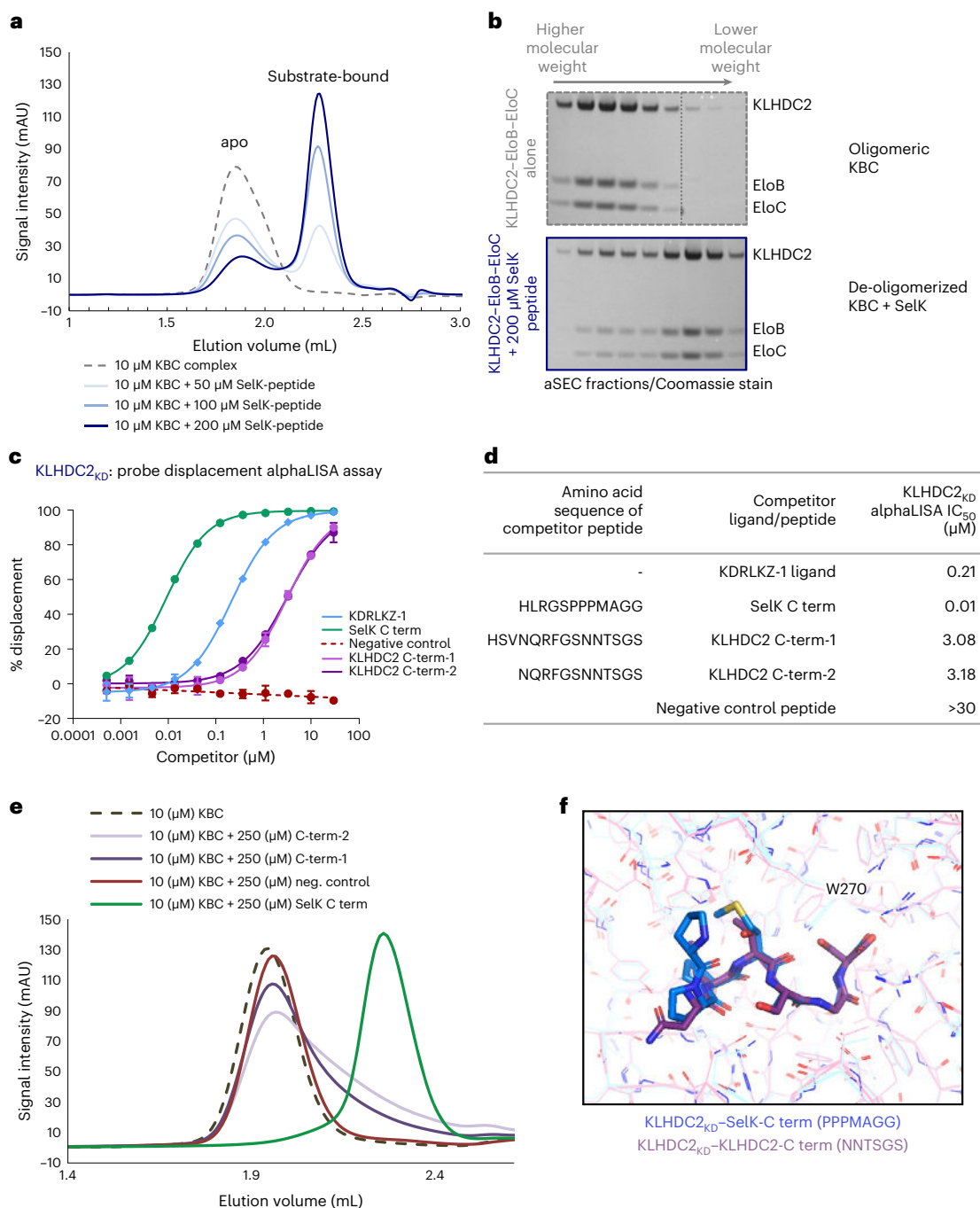


**Fig. 4 | Purified full-length KLHDC2–EloB–EloC<sub>3</sub> ligase complex is a dynamic oligomer held together in part by its own C termini.** **a**, Analytical size-exclusion chromatography (aSEC) traces of purified, full-length KBC complexes (at 10 μM) with increasing concentrations of a substrate peptide (SelK C terminus). **b**, SDS–PAGE analysis of aSEC fractions from **a** of 10 μM KBC alone (top) or 10 μM KBC incubated with 200 μM SelK peptide (bottom). The dotted line marks where the gel was cropped (representative gels shown of three biological replicates). **c, d**, Activities of short C-terminal peptides in the KLHDC2<sub>KD</sub> alphaLISA displacement assay, showing low but measurable displacement (**c**), with the IC<sub>50</sub> values listed in the table (**d**); *n* = 2 technical

replicates of 2 independent biological replicates are shown, and data are shown as mean ± s.d. **e**, aSEC traces of KBC complexes incubated with the indicated peptides, showing peak-broadening when KLHDC2 is incubated with peptides derived from its own C terminus *in trans*. **f**, X-ray crystal structure of a C-terminal KLHDC2 peptide bound to KLHDC2<sub>KD</sub> (PDB 8SGF, purple), overlaid with the crystal structure of the SelK C-terminal peptide bound to KLHDC2<sub>KD</sub> (PDB 6DO3, blue). This overlay highlights the substrate-binding pocket of KLHDC2, revealing the alignment between the two C-terminal peptides. KLHDC2<sub>KD</sub> is shown as lines, and C-terminal peptides are shown as sticks; Trp270 of KLHDC2 is labeled).

their ability to dissociate KBC tetramers as measured by analytical size-exclusion chromatography (Fig. 5d and Extended Data Fig. 7d). We also note that KLHDC2 ligands with longer half-lives, as measured by SPR kinetics, tended to induce more pronounced tetramer dissociation (Fig. 5d, table). Overall, our data are consistent with a model in which

apo-KBC is held together via its own C terminus, and substrates and small molecules (ligands or PROTACs) must gain access to individual KLHDC2 substrate-binding pockets to disrupt the tetramer and induce formation of dimers or monomers, ultimately leading to their active forms in complex with CRL2 (Fig. 5e).

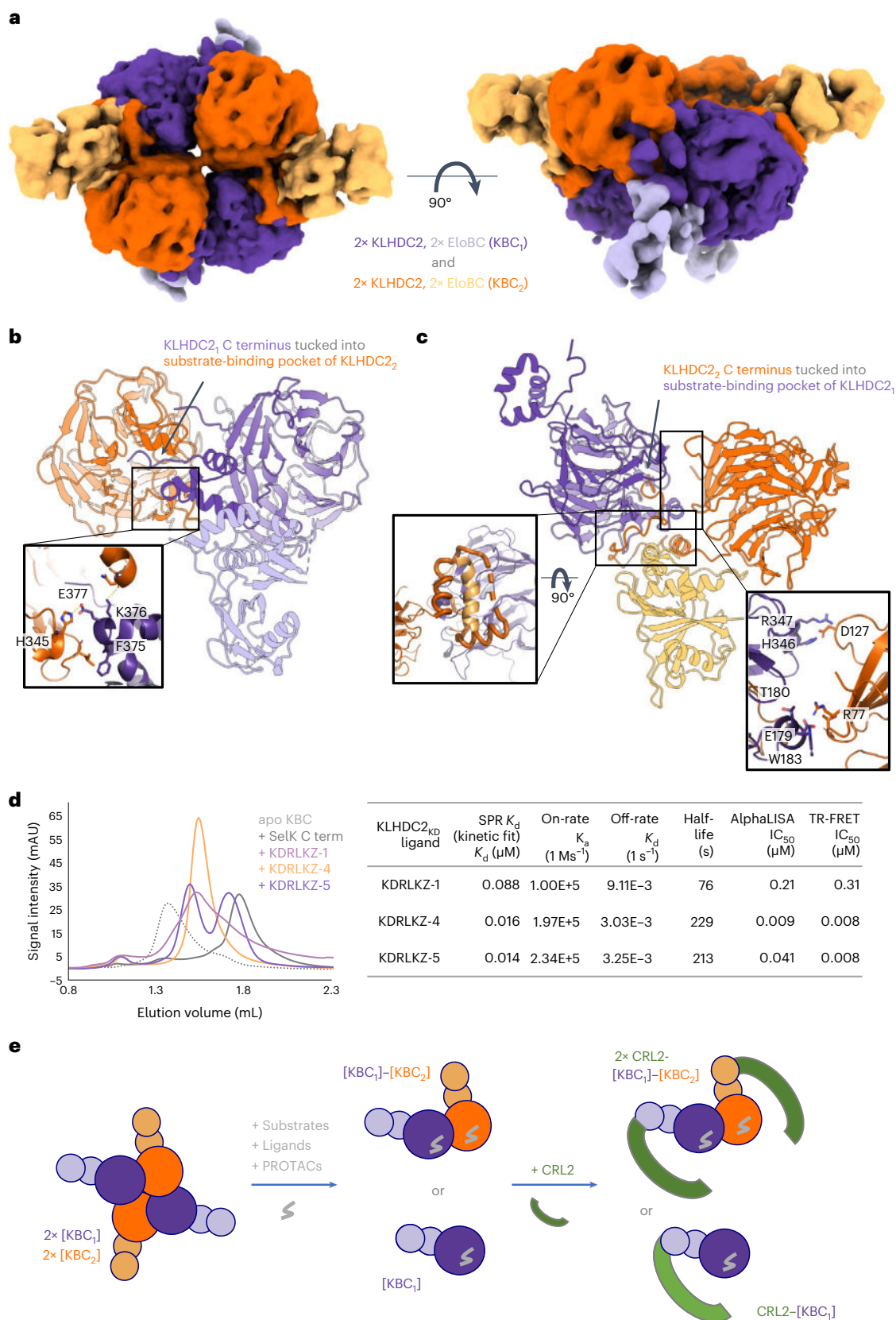


**Fig. 5 | Cryo-EM structure at 3.8 Å of the full-length, apo-KLHDC2-EloB-EloC complex reveals a tetramer. a**, Final map obtained by cryo-EM of the KBC tetramer in two orientations, revealing four copies of KLHDC2, EloB, and EloC each in the complex (PDB 8SH2, EMD-40477). **b**, Ribbon representation of the KLHDC2<sub>1</sub> C terminus binding the adjacent KLHDC2<sub>2</sub> kelch domain (see text for details on inserts). **c**, Ribbon representation of KLHDC2<sub>2</sub> C terminus binding the

adjacent KLHDC2<sub>1</sub> kelch domain (see text for details on inserts). **d**, aSEC traces of KBC complexes incubated with KLHDC2 small-molecule ligands, with their biochemical binding affinities shown in the table. **e**, Proposed model for KBC de-oligomerization and CRL2 binding upon engagement of KLHDC2 substrate-binding pockets by substrates or small molecules.

**Table 2 | Cryo-EM data collection, refinement, and validation statistics**

apo-KLHDC2-EloB-EloC (EMDB-40477, PDB 8SH2)	
Data collection and processing	
Magnification	×105,000
Voltage (kV)	300
Electron exposure (e <sup>-</sup> /Å <sup>2</sup> )	58.1
Defocus range (μm)	-1 to -2.5
Pixel size (Å)	0.83
Symmetry imposed	C <sub>2</sub>
Initial particle images (no.)	4,153,896
Final particle images (no.)	185,914
Map resolution (Å)	3.74
FSC threshold	0.143
Map resolution range (Å)	3.7 to 9.5
Refinement	
Initial model used (PDB code)	KLHDC2_AF-Q9Y2U9-F1-model_V4.pdb; PDB 5T35
Model resolution (Å)	3.74
FSC threshold	0.143
Model resolution range (Å)	3.7 to 9.5
Map sharpening B factor (Å <sup>2</sup> )	337.41
Model composition	
Non-hydrogen atoms	18,038
Protein residues	2,254
B factors (Å <sup>2</sup> )	
Protein	337.41
R.m.s. deviations	
Bond lengths (Å)	0.006
Bond angles (°)	1.197
Validation	
MolProbity score	2.0
Clashscore	14.5
Poor rotamers (%)	0.35
Ramachandran plot	
Favored (%)	95.21
Allowed (%)	4.79
Disallowed (%)	0.00

## Discussion

TPD relies on using engineered small molecules to co-opt E3 ligases to induce degradation of targets that are not natural substrates of said E3 ligases<sup>5</sup>. The technology of PROTAC heterobifunctional degraders offers a modular approach to TPD that allows matching of select E3 ligases and targets by linking their respective small-molecule ligands<sup>4</sup>. The most widely employed E3 ligases for TPD, including PROTAC degraders at the clinical stage<sup>29</sup>, are CRBN and VHL. However, there is widespread interest in expanding the scope of TPD by identifying more E3 ligases that can be used for this purpose<sup>2,6,12,14,30</sup>.

Achieving this goal, of course, will require identification of ligands that bind specific E3 ligases. Furthermore, understanding how an E3 ligase recognizes its native substrates is an important aspect of ligand-identification strategies. Other E3 ligase attributes, such as their

expression levels in tissues or cell lines and their tumor-enrichment profiles, can also be guiding factors in considering untapped E3 ligases<sup>2</sup>. Although a defined structure is not required for discovery of E3 ligands, it is an advantage. Highly active E3 ligases that target substrates for degradation in diverse settings, and whose substrate recognition has been elucidated at the structural level by X-ray crystallography (for example, KLHDC2 and other E3 ligases that recognize N- and C-terminal degrons) are ideal starting points in small-molecule ligand discovery. Successful ligand discovery then enables investigation of whether an E3 ligase can be functionally co-opted by heterobifunctional small molecules to recruit and degrade non-native targets (defined as 'E3 PROTACability'). Recruitment and degradation of BRD4, a commonly used model substrate for TPD, often comprise the first case study in establishing the PROTACability of an E3 ligase. Proteomics analysis after PROTAC treatment would shed further light on the specificity of KLHDC2-BRD4 degraders, and we show that they can degrade a related BET-family member, BRD2, much like the behavior of other PROTAC molecules linked to E3 ligases. Indeed, recent studies have demonstrated that BRD4 can be degraded by a handful of E3 ligases that can be used in TPD (for example, KEAP1, FEM1B, and DCAF11, as reviewed elsewhere<sup>31</sup>). The current work adds KLHDC2 to the list of ligandable E3 ligases. We report structure-based discovery of high-affinity small molecules that target the substrate-binding pocket of KLHDC2, and which enable generation of heterobifunctional PROTAC degrader molecules that induce BRD4 and AR degradation in a KLHDC2-dependent manner, thus establishing the PROTACability of KLHDC2.

Supporting KLHDC2 as an E3 ligase suited for PROTAC-mediated degradation, a recent proteome-wide study that profiled proximity-dependent modulation of protein stability across several substrates<sup>32</sup> has shown that KLHDC2 is an E3 ligase that can promote degradation of targets through induced proximity via engineered E3 fusions. It has therefore been suggested to be an ideal E3 ligase for TPD applications. Similarly, another recent study has demonstrated that KLHDC2 is an efficient degrader of multiple targets—such as STK33, KRas, and FoxP3—through induced proximity as well<sup>33</sup>. Here, the authors demonstrated, via peptide-based PROTAC-like molecules using HaloTag applications, that KLHDC2 recruitment by C-terminal peptides can result in target degradation. Finally, another recent study demonstrated that KLHDC2 recruitment via 'half-TAC' molecules (that is, a chimeric fusion of a SelK peptide and a promiscuous kinase war-head) led to the degradation of multiple kinases<sup>34</sup>.

Overall, given the native activity of KLHDC2 as a highly active E3 ligase that recognizes C-terminal degrons, and the studies that describe how KLHDC2 can be co-opted to degrade targets via induced proximity—including this work, which demonstrates small-molecule-based co-opting of KLHDC2 against two target classes—a picture is emerging of the potential utility of KLHDC2 in TPD.

In addition, this work reveals a structural model of a KLHDC2 tetramer that is modulated by the engagement of its substrate-binding pocket. It is tempting to speculate on what may control KLHDC2 dynamics in cells, but the distribution of endogenous KLHDC2 species—tetramers, dimers, and monomers, which can be bound to CRL2 or unbound—is not yet fully understood. However, it is now recognized that KLHDC2 and other E3 ligases targeting C-terminal degrons are highly active and shape the repertoire of proteomes by rapidly ubiquitylating proteins with Gly-terminating C termini, targeting them for proteasomal degradation<sup>35</sup>.

E3 ligase assembly into oligomers can represent a form of E3 regulation, and there are E3 ligases that function via dynamic assembly and disassembly into oligomers<sup>36</sup>. Oligomerization has been shown to modulate protein half-lives<sup>37</sup>, including CRL-type E3 ligase substrate adapters that are known to undergo autoubiquitylation<sup>38</sup>. For CRL substrate adapters, the half-life can be dependent on their CRL occupancy as well as by engagement of their substrates<sup>39</sup>. KLHDC2 has been observed to be in its activated state across cell types, as measured by the

relative abundance of KLHDC2 (and other substrate adapters) bound to activated CRLs<sup>40</sup>. This is consistent with the idea that substrate availability—or, simply, engagement of a substrate-binding pocket of a CRL substrate adapter—can dictate the activity of a substrate adapter by modulating its association with its cognate CRL. This has been demonstrated by studies from the Deshaies and Schulman labs<sup>39,40</sup>, which have shown that not only substrate adapter engagement by natural substrates of E3 ligases, but also engagement by small molecules and PROTAC degraders that target these substrate adapters, leads to increased E3 ligase CRL engagement and activity. Specifically for KLHDC2, this is consistent with recent overexpression studies showing that exogenously expressed KLHDC2 is subject to autoubiquitylation, but this could be modulated by substrate binding<sup>41</sup>.

Our observations and hypotheses are entirely consistent with a recent publication that has also deconvoluted KLHDC2 assembly<sup>41</sup>. Scott et al. similarly relied on structural biology and biochemical assays to reveal the tetrameric assembly of KLHDC2. Although the crystal structure presented by Scott et al. differs slightly from the cryo-EM structure presented here, in essence, both structures are consistent with the hypothesis that KLHDC2 is a dynamic oligomer with some flexibility in assembly. They extend this model to other C-terminal-degron E3 ligases, such as KLHDC3 (which they show is an oligomer as well), but not to KLHDC10 (which they show is a monomer; its own C terminus does not allow engagement of its substrate-binding pocket). The observation that ligands with longer half-lives induced greater dissociation of the KBC tetramer when engaging the substrate-binding pocket also aligns with the hypothesis from the Scott et al. paper: endogenous substrates—or newly recruited targets via heterobifunctional molecules—must efficiently disengage the KBC tetramer.

Altogether, the work described herein details identification of high-affinity small molecules targeting KLHDC2 that can be used to co-opt KLHDC2 for TPD, exemplified by degradation of BET-family proteins and the AR by KLHDC2-based heterobifunctional PROTAC degraders. We not only demonstrate how KLHDC2 can be co-opted by small molecules, but also describe dynamic KLHDC2 assembly and corroborate recent findings on its tetrameric form. To our knowledge, the non-covalent small molecules and PROTAC degraders described in this work represent the first example of targeting the substrate-binding pocket of a C-terminal-degron E3 ligase and hijacking it for TPD. Our findings introduce small-molecule tools that will allow future studies of the biology and mechanism of C-terminal-degron ligases, such as KLHDC2. These findings expand the field of induced proximity by enabling a hitherto untapped E3 ligase for potential TPD applications, including interrogation of its potential to target additional substrates for degradation.

## Online content

Any methods, additional references, Nature Portfolio reporting summaries, source data, extended data, supplementary information, acknowledgements, peer review information; details of author contributions and competing interests; and statements of data and code availability are available at <https://doi.org/10.1038/s41594-023-01146-w>.

## References

- Ciechanover, A., Orian, A. & Schwartz, A. L. Ubiquitin-mediated proteolysis: biological regulation via destruction. *Bioessays* **22**, 442–51 (2000).
- Békés, M., Langley, D. R. & Crews, C. M. PROTAC targeted protein degraders: the past is prologue. *Nat. Rev. Drug Discov.* **21**, 181–200 (2022).
- Komander, D. & Rape, M. The ubiquitin code. *Annu. Rev. Biochem.* **81**, 203–29 (2012).
- Sakamoto, K. M. et al. Protacs: chimeric molecules that target proteins to the Skp1-Cullin-F box complex for ubiquitination and degradation. *Proc. Natl Acad. Sci. USA* **98**, 8554–9 (2001).
- Faust, T. B., Donovan, K. A., Yue, H., Chamberlain, P. P. & Fischer, E. S. Small-molecule approaches to targeted protein degradation. *Annu. Rev. Cancer Biol.* **5**, 181–201 (2021).
- Ishida, T. & Ciulli, A. E3 ligase ligands for PROTACs: how they were found and how to discover new ones. *SLAS Discov.* **26**, 484–502 (2020).
- Harper, J. W. & Schulman, B. A. Cullin-RING ubiquitin ligase regulatory circuits: a quarter century beyond the F-box hypothesis. *Annu. Rev. Biochem.* **90**, 1–27 (2021).
- Lin, H.-C. et al. C-terminal end-directed protein elimination by CRL2 ubiquitin ligases. *Mol. Cell* **70**, 602–613 (2018).
- Koren, I. et al. The eukaryotic proteome is shaped by E3 ubiquitin ligases targeting C-terminal degrons. *Cell* **173**, 1622–1635 (2018).
- Meszaros, B., Kumar, M., Gibson, T. J., Uyar, B. & Dosztanyi, Z. Degrons in cancer. *Sci. Signal* **10**, eaak9982 (2017).
- Rusnac, D. V. et al. Recognition of the glycine C-end degron by CRL2<sup>KLHDC2</sup> ubiquitin ligase. *Mol. Cell* **72**, 813–822 (2018).
- Jevtić, P., Haakonsen, D. L. & Rapé, M. An E3 ligase guide to the galaxy of small-molecule-induced protein degradation. *Cell Chem. Biol.* **28**, 1000–1013 (2021).
- Bricelj, A., Steinebach, C., Kuchta, R., Gütschow, M. & Sosić, I. E3 ligase ligands in successful PROTACs: an overview of syntheses and linker attachment points. *Front. Chem.* **9**, 707317 (2021).
- Kannt, A. & Đikić, I. Expanding the arsenal of E3 ubiquitin ligases for proximity-induced protein degradation. *Cell Chem. Biol.* **28**, 1014–1031 (2021).
- Buckley, D. L. et al. Targeting the von Hippel-Lindau E3 ubiquitin ligase using small molecules to disrupt the VHL/HIF-1 $\alpha$  interaction. *J. Am. Chem. Soc.* **134**, 4465–4468 (2012).
- Dobrodziej, J. et al. Evaluating ligands for ubiquitin ligases using affinity beads. *Methods Mol. Biol.* **2365**, 59–75 (2021).
- Filippakopoulos, P. et al. Selective inhibition of BET bromodomains. *Nature* **468**, 1067–1073 (2010).
- Riching, K. M. et al. Quantitative live-cell kinetic degradation and mechanistic profiling of PROTAC mode of action. *ACS Chem. Biol.* **13**, 2758–2770 (2018).
- Zou, Y., Rojas-Pierce, M., Raikhel, N. V. & Pirrung, M. C. Preparation of methyl ester precursors of biologically active agents. *Biotechniques* **44**, 377–384 (2008).
- Raina, K. et al. PROTAC-induced BET protein degradation as a therapy for castration-resistant prostate cancer. *Proc. Natl Acad. Sci. USA* **113**, 7124–7129 (2016).
- Ohba, K. Sulfonamide or sulfonamide compound having effect of inducing BRD4 protein degradation and pharmaceutical use thereof. World Intellectual Patent Organization WO/2021/157684 (2021).
- Li, Y.-D. et al. Template-assisted covalent modification of DCAF16 underlies activity of BRD4 molecular glue degraders. Preprint at biorXiv <https://doi.org/10.1101/2023.02.14.528208> (2023).
- Hsia, O. et al. An intramolecular bivalent degrader glues an intrinsic BRD4–DCAF16 interaction. Preprint at biorXiv <https://doi.org/10.1101/2023.02.14.528511> (2023).
- Pla-Prats, C., Cavadini, S., Kempf, G. & Thomä, N. H. Recognition of the CCT5 di-Glu degron by CRL4DCAF12 is dependent on TRiC assembly. *EMBO J.* **42**, e112253 (2023).
- Canzani, D., Rusnac, D.-V., Zheng, N. & Bush, M. F. Degronomics: mapping the interacting peptidome of a ubiquitin ligase using an integrative mass spectrometry strategy. *Anal. Chem.* **91**, 12775–12783 (2019).
- Punjani, A. & Fleet, D. J. 3D variability analysis: resolving continuous flexibility and discrete heterogeneity from single particle cryo-EM. *J. Struct. Biol.* **213**, 107702 (2021).
- Punjani, A., Zhang, H. & Fleet, D. J. Non-uniform refinement: adaptive regularization improves single-particle cryo-EM reconstruction. *Nat. Methods* **17**, 1214–1221 (2020).

28. Nguyen, H. C., Yang, H., Fribourgh, J. L., Wolfe, L. S. & Xiong, Y. Insights into Cullin–RING E3 ubiquitin ligase recruitment: structure of the VHL–EloBC–Cul2 complex. *Structure* **23**, 441–449 (2015).
29. Chirnomas, D., Hornberger, K. R. & Crews, C. M. Protein degraders enter the clinic—a new approach to cancer therapy. *Nat. Rev. Clin. Oncol.* **20**, 265–278 (2023).
30. Schapira, M., Calabrese, M. F., Bullock, A. N. & Crews, C. M. Targeted protein degradation: expanding the toolbox. *Nat. Rev. Drug Discov.* **18**, 949–963 (2019).
31. Lee, J. et al. Discovery of E3 ligase ligands for target protein degradation. *Molecules* **27**, 6515 (2022).
32. Poirson, J. et al. Proteome-scale induced proximity screens reveal highly potent protein degraders and stabilizers. Preprint at biorXiv <https://doi.org/10.1101/2022.08.15.503206> (2022)
33. Röth, S. et al. Screening of E3 ligases uncovers KLHDC2 as an efficient proximity-induced degrader of K-RAS, STK33,  $\beta$ -catenin and FoxP3. *SSRN Electron J.* <https://doi.org/10.2139/ssrn.4214930> (2022).
34. Kim, Y. et al. Targeted kinase degradation via the KLHDC2 ubiquitin E3 ligase. *Cell Chem Biol* <https://doi.org/10.1016/j.chembiol.2023.07.008> (2023)
35. Sherpa, D., Chrustowicz, J. & Schulman, B. A. How the ends signal the end: regulation by E3 ubiquitin ligases recognizing protein termini. *Mol. Cell.* **82**, 1424–1438 (2022).
36. Balaji, V. & Hoppe, T. Regulation of E3 ubiquitin ligases by homotypic and heterotypic assembly. *F1000Res.* **9**, F1000 Faculty Rev-88 (2020).
37. Mallik, S. & Kundu, S. Topology and oligomerization of mono- and oligomeric proteins regulate their half-lives in the cell. *Structure* **26**, 869–878 (2018).
38. Mohamed, W. I. et al. The CRL4DCAF1 Cullin–RING ubiquitin ligase is activated following a switch in oligomerization state. *EMBO J.* **40**, e108008 (2021).
39. Reichermeier, K. M. et al. PIKES analysis reveals response to degraders and key regulatory mechanisms of the CRL4 network. *Mol. Cell* **77**, 1092–1106 (2020).
40. Henneberg, L. T. et al. Activity-based profiling of cullin–RING ligase networks by conformation-specific probes. *Nat Chem Biol* <https://doi.org/10.1038/s41589-023-01392-5> (2023)
41. Scott, D. C. et al. E3 ligase autoinhibition by C-degron mimicry maintains C-degron substrate fidelity. *Mol. Cell* **83**, 770–786 (2022).

**Publisher's note** Springer Nature remains neutral with regard to jurisdictional claims in published maps and institutional affiliations.

Springer Nature or its licensor (e.g. a society or other partner) holds exclusive rights to this article under a publishing agreement with the author(s) or other rightsholder(s); author self-archiving of the accepted manuscript version of this article is solely governed by the terms of such publishing agreement and applicable law.

© The Author(s), under exclusive licence to Springer Nature America, Inc. 2024

## Methods

### Protein expression and purification

Cul2 and Rbx1 were prepared as previously described<sup>42</sup>. Briefly, His-MBP-TEV-Cul2 (1-745) (Uniprot: [Q13617](#)) and Rbx1 (Uniprot: [P62877](#)) were co-expressed from a pFastBacDual1 vector in Sf21 cells. Collected cells were lysed by stirring in buffer containing 50 mM Hepes pH 8.0, 250 mM NaCl, 10 mM imidazole, 2 mM TCEP, 1% Triton X-100, and protease inhibitor tablets (Roche). The clarified lysate was applied to a HisTrap FF Crude column and washed with 50 mM Hepes pH 8.0, 250 mM NaCl, 10 mM imidazole, 2 mM TCEP, and 5% glycerol. Protein was eluted with wash buffer supplemented with 300 mM imidazole. This pool was incubated with TEV protease for 5 h at 4 °C in dialysis buffer containing 50 mM Hepes pH 8.0, 100 mM NaCl, 10 mM imidazole, 2 mM TCEP, and 5% glycerol. The cleaved pool was added to a HisTrap column for reverse-affinity chromatography, and the flow-through was collected and concentrated for subsequent size-exclusion chromatography. Protein was added to a S200 26/60 column pre-equilibrated with dialysis buffer lacking imidazole. Pure fractions containing Cul2 and Rbx1 were brought to a concentration of 1.5 mg mL<sup>-1</sup> and flash-frozen for storage at -80 °C.

A gene encoding full-length KLHDC2 (Uniprot: [Q9Y2U9](#)) with an N-terminal GST-TEV-His tag was synthesized (Genscript) and cloned into a pFastBac vector. Full-length EloB (Uniprot: [Q15370](#)) and EloC (Uniprot: [Q15369](#)) were synthesized (Genscript) and cloned into multiple cloning sites of pFastBacDual. KLHDC2, EloB, and EloC were co-expressed in Sf21 cells. Collected cells were lysed by gentle stirring in lysis buffer containing 20 mM Tris pH 8.0, 200 mM NaCl, 5 mM DTT, and protease inhibitors. The clarified lysate was applied to Pierce glutathione agarose beads overnight and washed with lysis buffer without protease inhibitors. TEV was added to the slurry for overnight digestion at 4 °C, and the resulting flow-through contained both the KBC complex and TEV. These were easily separated on a HiLoad Superdex 200 26/600 column pre-equilibrated with 20 mM Tris pH 8.0, 200 mM NaCl, and 1 mM TCEP. Pure fractions were concentrated and flash-frozen for storage at -80 °C.

The kelch domain of KLHDC2 (KLHDC2<sub>KD</sub>) was purified as previously described with minor modifications<sup>11</sup>. A gene encoding His-TEV-KLHDC2 (1-362) was cloned into pFastBac and expressed in Sf21 cells. Collected cells were lysed by sonication in buffer containing 50 mM Hepes pH 7.5, 250 mM NaCl, 10 mM imidazole, 1 mM TCEP, and protease inhibitor tablets (Roche). The clarified lysate was applied to a HisTrap FF Crude column and washed with 50 mM Hepes pH 7.5, 200 mM NaCl, and 1 mM TCEP. Protein was eluted with wash buffer supplemented with 500 mM imidazole. For crystallography, this pool was incubated with TEV protease for 5 h at 4 °C in dialysis buffer containing 50 mM Hepes pH 7.5, 100 mM NaCl, and 1 mM TCEP. The cleaved or uncleaved proteins were diluted fivefold with 20 mM Tris pH 8.0 and 1 mM TCEP, and were loaded onto a HiTrap Q column. Protein was eluted over a gradient of 20 mM Tris pH 8.0, 1 M NaCl, and 1 mM TCEP. Peak fractions were collected and concentrated for subsequent size-exclusion chromatography. Protein was added to a S200 26/60 column that was pre-equilibrated with 20 mM Tris, pH 8.0, 200 mM NaCl, and 1 mM TCEP. Pure fractions were concentrated and flash-frozen for storage at -80 °C. GST-KLHDC2<sub>KD</sub> was purified as previously described<sup>11</sup>.

His-tagged VHL-EloB-EloC was purified as previously described with a few modifications<sup>43</sup>. His-TEV-VHL (1-213) (Uniprot: [P40337](#)) was synthesized (Genscript) and cloned into a pET28a vector. EloB (1-118) and EloC (17-112) were synthesized (Genscript) and cloned into a pCDF-Duet vector. Both clones were co-transformed into BL21(DE3) cells, grown overnight at 37 °C in 5 mL Luria Broth supplemented with 50 µg mL<sup>-1</sup> each of kanamycin and streptomycin. The next morning, overnight culture was amplified into 6 L of terrific broth supplemented with kanamycin and streptomycin. Cells were grown at 37 °C at 200 r.p.m. to an optical density at 600 nm of 0.6. At that point, IPTG was added to a final concentration of 0.5 mM. Cells were incubated at 25 °C overnight with shaking at 200 r.p.m. Collected cells were resuspended

in 50 mM Tris pH 8, 300 mM NaCl, and 1 mM TCEP and lysed by two passes through the Emulsiflex at 15,000 psi. Lysate was clarified by spinning at 13,500 r.p.m. (22,000g) in a SS-34 rotor for 30 min at 4 °C. Clarified lysate was added to a gravity cobalt column. The column was washed with 50 mM Tris pH 8, 300 mM NaCl, 1 mM TCEP, 10 mM imidazole, and product elution was performed with wash buffer supplemented with 250 mM imidazole. This was concentrated and loaded onto a HiLoad S200 prep grade 16/60 column that was pre-equilibrated with 50 mM Hepes pH 7.5, 300 mM NaCl, 1 mM TCEP. Pure fractions were concentrated and flash-frozen for storage at -80 °C.

### Computer-aided drug design and molecular modeling

The de novo design of KLHDC2 ligands started with the KLHDC2–SelK peptide X-ray structure (PDB [6DO3](#), chains B and D). The protein complex was set up for modeling within the Schrodinger Maestro<sup>44</sup> package using the Protein Preparation Wizard<sup>45</sup>. Compounds were hand built within the pocket and optimized using Embrace Minimization. The compounds with the best Embrace Minimization scores were further evaluated for MD stability over a 100-ns simulation using Desmond<sup>46</sup>. MD scoring was used for evaluation only if the newly designed interaction was maintained for at least 50% of the time in the simulation.

### Synthesis of ligands and PROTACs

All synthetic chemistry methods are described in the Supplementary Methods.

### KLHDC2 alphaLISA and TR-FRET displacement assays

Compounds or peptides were tested in dose–response experiments to assess their ability to disrupt the KLHDC2–SelK peptide interaction in both alphaLISA and TR-FRET assays, both of which were performed in duplicates. In the alphaLISA assay, compounds were tested in a 384-well format with 30 µL total volume in each well. The final reactions included 3 nM 6×His-KLHDC2<sub>KD</sub>, 2 nM biotinylated SelK peptide (biotin-HLRGSPPMAGG, Genscript), 12.5 µg mL<sup>-1</sup> Anti-6×His Acceptor Beads (PerkinElmer), and 12.5 µg mL<sup>-1</sup> Streptavidin Donor Beads (PerkinElmer), and varying concentrations of compound, which was added to achieve a final concentration of 1.0% DMSO in buffer consisting of 50 mM HEPES (pH 7.4), 50 mM NaCl, 69 µM Brij-L23 (Sigma), and 0.1 mg mL<sup>-1</sup> BSA (Sigma) in white 384-well microtiter plates. Briefly, 12 µL of 6×-KLHDC2<sub>KD</sub>–biotin–SelK peptide and 3 µL of the compound dilution series were incubated at room temperature for 15 min, which was followed by the addition of 7.5 µL Anti-6×His Acceptor Beads and incubation for an additional 15 min. Then, 7.5 µL of Streptavidin Donor beads was added, and the reaction mixture was incubated for 15 min. AlphaLISA measurements (excitation 680 nm, emission 615 nm) were performed using an Envision plate reader (PerkinElmer). Data were normalized to the untreated neutral control (NC), representing 0% activity or displacement, and the condition when no protein was added represented 100% activity or displacement. The IC<sub>50</sub> was calculated using four-parameter logarithmic curve fitting in Prism. For the TR-FRET assay, compounds were tested in dose–response experiments for their ability to disrupt the KLHDC2–SelK peptide interaction in 384-well format, with final concentrations in each well of 15 µL total volume, 0.8 nM 6×His-KLHDC2<sub>KD</sub>, 6.67 nM anti-His-D2 (CisBio), 0.57 nM biotinylated SelK peptide (biotin-HLRGSPPMAGG), 0.25 nM streptavidin-terbium (CisBio), and varying concentrations of compound, which was added to achieve a final 0.5% DMSO concentration in buffer consisting of 25 mM HEPES, pH 7.5, 100 mM NaCl, 1 mM TCEP, 0.01% Tween-20, and 0.005% BSA (Sigma) in low-volume white 384-well microtiter plates (PerkinElmer ProxiPlate). Briefly, 5 µL of 6×His-KLHDC2<sub>KD</sub>–anti-HisD2 mixture and 5 µL of the compound dilution series were incubated at room temperature for 20 min, followed by the addition of 5 µL Biotin–SelK peptide–streptavidin-d2 mixture, and an additional 60-min incubation. TR-FRET (excitation 320 nm, emission 665 nm, emission 620 nm) was measured on an Envision (PerkinElmer)

or Pherastar Plus (BMG Labtech) multimode plate reader, and the ratio between the emission intensity at 665 nm and the emission intensity at 620 nm was calculated. Data were normalized to the untreated NC, representing 0% activity, and the inhibitor positive control (PC) (10  $\mu\text{M}$  KDKRLZ-1, or no protein added), representing 100% activity, and the  $\text{IC}_{50}$  was calculated using four-parameter logarithmic curve fitting in Prism. In tables, where applicable, geometric means are shown for the  $\text{IC}_{50}$ , with a minimum of two independent replicates. Peptides for the displacement assay were synthesized by Genscript.

### VHL alphaLISA displacement assays

Compounds were tested in dose–response experiments to assess their ability to disrupt VHL–biotinylated small molecule probe (or Hif-1- $\alpha$  peptide) interaction in alphaLISA in duplicate. For alphaLISA, compounds were tested in a 384-well format with 30  $\mu\text{L}$  total volume in each well, and final concentrations of 12 nM His-VHL-EloB/C complex, 30 nM biotinylated probe, 12.5  $\mu\text{g mL}^{-1}$  Anti-6 $\times$ His Acceptor Beads (PerkinElmer), and 12.5  $\mu\text{g mL}^{-1}$  Streptavidin Donor Beads (PerkinElmer), and varying concentrations of compound, which was added to achieve a final concentration of 1.0% DMSO in buffer consisting of 50 mM HEPES (pH 7.4), 50 mM NaCl, 69  $\mu\text{M}$  Brij-L23 (Sigma), and 0.1 mg  $\text{mL}^{-1}$  BSA (Sigma) in white 384-well microtiter plates. Briefly, 12  $\mu\text{L}$  of His-VHL+EloB/C–biotin probe and 3  $\mu\text{L}$  of the compound dilution series were incubated at room temperature for 15 min, which was followed by the addition of 7.5  $\mu\text{L}$  Anti-6 $\times$ His Acceptor Beads and incubated an additional 15 min. Then, 7.5  $\mu\text{L}$  of Streptavidin Donor Beads were added, and the reaction mixture was incubated for a final 15 min. AlphaLISA (excitation 680 nm, emission 615 nm) was measured on an Envision plate reader (Perkin Elmer). Data were normalized to the untreated NC, representing 0% activity or displacement, and the condition when no protein was added represented 100% activity or displacement. The  $\text{IC}_{50}$  was calculated using four-parameter logarithmic curve fitting in Prism. In tables, where applicable, geometric means are shown for  $\text{IC}_{50}$ , with a minimum of two independent replicates.

### SPR binding experiments with KLHDC2<sub>KD</sub> and ternary-complex SPR assay

All measurements of direct binding in SPR experiments were collected using the Biacore 8K+ instrumentation, and ternary-complex binding measurements were collected using the BiacoreS200 (Cytiva). For direct-binding measurements, His-TEV-KLHDC2<sub>KD</sub> was immobilized using direct coupling of protein (Cytiva BR100223) to an NTA sensor chip (Cytiva 28994951), according to the kit's protocol. Flow cell 1 was activated or deactivated to provide a reference surface, and all eight channels of flow cell 2 were used for binding analysis. The targeted immobilization level across all channels was at least 4,000 RU. After immobilization, the sensor surface was primed with SPR running buffer containing 2% DMSO and allowed to equilibrate for 3 h. SPR running buffer consists of 50 mM Tris HCl, pH 7.5 (Invitrogen 15567-027), 250 mM NaCl (Sigma Life Science 101988757), 0.05% P20 (Cytiva BR100671), 1 mM dithiothreitol (Sigma Aldrich 646563), 0.1 mg  $\text{mL}^{-1}$  BSA (Sigma Aldrich 3311), and 2% DMSO (vol/vol) (Sigma Aldrich 2766855). Compounds were diluted in threefold dilutions (11 data points and a control were collected (11-point + blank)) in 384-well plates, with the maximum concentrations ranging from 2.5 mM to 10 mM in 100% DMSO. Two microliters of this solution was dispensed into a 384-well plate and further diluted to a final volume of 100  $\mu\text{L}$  with SPR running buffer (without DMSO), resulting in final maximum concentrations of 50–200  $\mu\text{M}$ . Compound binding was measured using multi-cycle analysis at a flow rate of 30  $\mu\text{L min}^{-1}$ , with association and dissociation phases each lasting 60 s.

For ternary-complex binding measurements, His-BRD4 (amino acids 342–460) was purchased from Sigma Aldrich (Sigma SRP0462) and immobilized using direct coupling of protein (Cytiva BR100223) to a NTA sensor chip (Cytiva 28994951), according to the kit's protocol.

Flow cells 1 and 2 were activated or deactivated to provide a reference surface, and flow cells 3 and 4 were used for binding analysis. The targeted immobilization level across all channels was at least 500 RU. After immobilization, the sensor surface was primed with SPR running buffer containing 2% DMSO and allowed to equilibrate for 3 h. SPR running buffer consists of 50 mM Tris HCl, pH 7.5 (Invitrogen 15567-027), 250 mM NaCl (Sigma Life Sciences 101988757), 0.1% P20 (Cytiva BR100671), 1 mM dithiothreitol (Sigma Aldrich 646563), 0.4 mg  $\text{mL}^{-1}$  BSSA (Sigma Aldrich 3311), and 2% DMSO (vol/vol) (Sigma Aldrich 2766855). Compounds were diluted with threefold dilutions (11-point + blank) in 384-well plates with maximum concentrations of 25–50  $\mu\text{M}$  in 100% DMSO. GST-TEV-KLHDC2<sub>KD</sub> was diluted in threefold dilutions (11-point + blank) in 384-well plates, with a maximum concentration of 18  $\mu\text{M}$  in SPR running buffer (without DMSO). Two microliters of the diluted compound solution and 5.5  $\mu\text{L}$  of the diluted GST-TEV-KLHDC2<sub>KD</sub> solution were co-spotted into a 384-well plate and further diluted to a final volume of 100  $\mu\text{L}$  with SPR running buffer (without DMSO), resulting in final equimolar maximum concentrations of 0.5–1  $\mu\text{M}$ . Compound binding was measured using multi-cycle analysis at a flow rate of 30  $\mu\text{L min}^{-1}$ , with the association phase lasting 90 s and the dissociation phase lasting 360 s. All compounds were tested as technical replicates within a given experiment, and the data reported are the average result of at least two independent experiments. Data underwent double reference subtraction and were DMSO-corrected. All binding data were analyzed using the Biacore Insight Evaluation Software (Cytiva) using multi-cycle affinity and kinetic evaluation. Binding  $K_d$  values were analyzed using affinity fitting, and ternary-complex binding was further analyzed using the Biacore Insight Evaluation Software (Cytiva) using multi-cycle kinetic evaluation. SPR binary kinetics were measured using the Biacore Insight Evaluation Software (Cytiva); kinetic evaluation and goodness of fit were determined using  $U$  values. The half-life was calculated using a standard first-order kinetic equation.  $K_d$  values are shown as geometric means, where applicable (minimum  $n = 2$ ).

### Thermal-shift measurements

Thermal-shift assays were carried out by monitoring the thermal melting curves of 13  $\mu\text{M}$  KLHDC2<sub>KD</sub> with SYPRO orange (Invitrogen S6650) in assay buffer containing 20 mM Tris, pH 8.0, 200 mM NaCl, and 2 mM TCEP in Microamp 96-well plates (N8010560 Applied Biosystems) with FG optical adhesive covers (4311971 Applied Biosystems). Assays were performed in triplicate with 100  $\mu\text{M}$  ligands on a Quantstudio 6 Real-time PCR machine, with 0.5° increments for 30 s from 25° to 95 °C.

### X-ray crystallography of KLHDC2<sub>KD</sub> with compounds or peptides

Apo-KLHDC2<sub>KD</sub> crystals were obtained by sitting drop vapor diffusion. Drops containing a 2:1 ratio of protein to mother liquor regularly produced 300  $\mu\text{m}$  cigar-shaped crystals at 18° C, with mother liquor containing 11 mM Tris pH 8.0, 8 mM hexamine cobalt, 260–450 mM NaCl, and 24–34% PEG-4000. Ligands and peptides were soaked at 1 mM for 24–72 h. Crystals were cryoprotected using 10% glycerol added to the mother liquor, and then were flash-frozen. Diffraction data were collected on an Advanced Photon Source IMCA-CAT beamline. All data sets were integrated and scaled with autoPROC<sup>47</sup>, and initial models were obtained by performing molecular replacement using PHASER<sup>48</sup> (initial model PDB 6DO3)<sup>41</sup>. The models were improved by iterative rounds of refinement using BUSTER (<https://www.globalphasing.com/buster>) and manual model building in COOT<sup>49,50</sup>. Ligand restraints were generated in Grade version 1.2.20 (Global Phasing)

### Affinity pull-down assays using biotin–ligand compounds

Protein affinity beads were generated using biotin-conjugated ligand compounds and streptavidin–agarose, as described previously<sup>16</sup>. PBS with 0.2% NP-40 alternative was used for extraction (with protease inhibitors) and bead washes. Proteins were eluted from beads using 1 $\times$  LDS sample buffer (Thermo). High-capacity streptavidin–agarose

(SA) was obtained from Thermo (20361). The antibody to KLHDC2 was obtained from Thermo (PA5-90252). Each pull-down assay used 40  $\mu$ L of SA slurry with 5  $\mu$ M ligand (using a 1 mL volume) and 1 mg of cell extract. Each lane was loaded with 87.5% of each eluate, and the input lane on the immunoblot had 10 mg of extract. For pull-down assays with a readout of the relative HiBiT signal, washed SA beads were resuspended in 80 mL Nano-Glo HiBiT Lytic Detection System reagent and transferred to wells of white 96-well plates, which was followed by measurements of luminescence on an Envision multimode plate reader.

### Cell-free ubiquitylation reactions

A peptide with sequence SKVLNKNVEAIGLLGG, derived from human USP1, and N-terminally labeled with Cy5 was synthesized by Genscript. Proteins, other than those listed above, were from R&D Systems: E1 (human Uba1), E2 (human UbcH5), and human ubiquitin. The assay buffer was composed of 25 mM HEPES (pH 7.5), 125 mM NaCl, 2 mM MgCl<sub>2</sub>, and 1 mM DTT. Equimolar ATP–MgCl<sub>2</sub> was added from a 100 mM stock (R&D Systems) to a final concentration of 2 mM, where indicated. Overnight reactions were terminated with a 4X custom gel loading buffer, having a final composition of: 50 mM Tris–Cl (pH 7.4), 10% glycerol, 2% SDS, and Orange G dye (to the desired color). Wet NuPAGE (Thermo) gels were imaged on a ChemiDoc MP (Bio-Rad) using the Cy5 setting. The same gels were then subjected to protein transfer onto a PVDF membrane using an iBlot2 apparatus. Immunoblots for ubiquitin used a primary antibody from Cell Signaling Technology (3933), a horseradish-peroxidase-linked secondary antibody, and enhanced chemiluminescence reagent, with image acquisition on ChemiDoc MP using the chemiluminescence setting.

### Cells and reagents

PC-3 cells were edited by CRISPR–Cas9 technology at Promega to express HiBiT-BRD4 from one of two chromosomal loci (CS3023130). These PC-3\_HiBiT-BRD4 cells were maintained in F-12K medium (ATCC 30-2004) supplemented with 10% FBS (Gibco). AD-293 cells were purchased from Agilent (240085) and grown in DMEM, high glucose, GlutaMAX, pyruvate medium (Gibco 10569044) supplemented with 10% FBS. Antibodies to the following proteins were from commercial suppliers: AR (CST 5153); BRD2 (CST, 5848); BRD4 (Abcam, ab243862); KLHDC2 (Thermo, PA5-90252); and tubulin (CST, 6074). The NAE inhibitor MLN-4924 was purchased from Sigma (5054770001). Additional cell lines (VCaP, PC-3, A549, A565, SK-BR-3) were purchased from ATCC and maintained and passaged according to their respective standard tissue-culture protocols.

### Target degradation assays

HiBiT-BRD4 levels were measured in 384-well plates using the Nano-Glo HiBiT Lytic Detection System (Promega N3050) in duplicates, with multiple independent runs. Cells were seeded at 5,000 cells per well, and compounds were added 16–24 h later using an Agilent BRAVO, with an intermediate dilution of compounds (stored in DMSO) into medium before dosing the compounds into the assay plates. After the indicated incubation times, plates were removed from the CO<sub>2</sub> incubator, Nano-Glo reagent was added to wells using either a multi-channel pipette or Multidrop Combi dispenser (Thermo), plates were incubated for 20–40 min at ambient temperature, and then plates were read for luminescence on an Envision multimode plate reader. GraphPad PRISM was used to generate graphs and to calculate DC<sub>50</sub> and  $D_{\max}$  values, using a four-parameter fit. Geometric means are shown for degradation characteristics (DC<sub>50</sub> and  $D_{\max}$ ) in the table in Figure 3d (minimum of  $n = 2$  repeats).

For experiments that involved both HiBiT levels and immunoblots of BRD proteins, HiBiT levels were measured using clarified cell extracts. In those cases, and in cases with only immunoblot readouts, cells were grown and treated in six-well plates and washed with DPBS, and proteins were extracted with RIPA buffer (Thermo 89900)

supplemented with protease inhibitors (Thermo 87786) and phosphatase inhibitors (Thermo 78420). After 15 min of extraction on ice, samples were transferred to 1.5-mL tubes and centrifuged at 21,130g in a tabletop microcentrifuge for 20 min at 4 °C. Supernatants were collected, and small aliquots of each sample were used to measure protein concentration by the BCA assay (Thermo) or HiBiT signal. Relative HiBiT levels were normalized to protein concentration. The remainder of each supernatant was processed for denaturing PAGE (NuPAGE; Thermo), followed by immunoblotting on PVDF membranes.

To measure AR levels, VCaP cells were seeded in 6-well plates in DMEM without phenol red (Gibco 31053028), supplemented with 10% FBS (Gibco), and were incubated for 2 d before the medium was changed to the same DMEM base medium but with 5% charcoal-stripped FBS (Gibco A33821-01). Compounds were diluted in the same medium and added to cells 24 h after the medium was changed. After 12 h of treatment with the compound, cell monolayers were processed for immunoblots as described above for BRD proteins, except the extraction buffer included benzonase (Sigma E1014). MLN-4924 was used at a concentration of 1  $\mu$ M.

### Nanoluc-degron cells and assays

DNA encoding nanoluc proteins with various C-terminal degron appendages was synthesized and cloned into a plasmid with an ampicillin resistance cassette (for bacterial selection), zeocin resistance cassette (for mammalian cell selection), and HSV-TK promoter (for gene expression in mammalian cells). These plasmids were linearized using the restriction enzyme PvuI and were transfected into AD-293 cells (Agilent), which was followed by selection of pools, and later by selection of clones, that were resistant to zeocin (Thermo). Cell pools and clones were selected on the basis of increases in levels of NLD proteins following treatment with UPS inhibitors, as measured using Nano-Glo Lytic reagent. A NLD clone expressing a nanoluc-degron (for KLHDC2) was tested with varying concentrations of MLN-4924 (Sigma). For gene knockdown experiments in clonal cells, siRNAs and transfection reagents (siTran 2.0) were obtained from OriGene: KLHDC2-A,B,C (SR308385); KLHDC3-A,B,C (SR314549); and KLHDC10-A,B,C (SR307932). These siRNAs were used at a final concentration of 50 nM.

### Genetic knockdown by siRNA

All experiments that included siRNA treatments outside of the arrayed siRNA library screen or NLD assays were conducted in six-well plates. The experiment shown in Extended Data Figure 2e used siRNA SR308385-B and transfection reagents from OriGene (see above and table below). The final concentration of siRNA, before compound dosing, was 50 nM. For the experiments shown in Figure 3f,g,j, the siRNAs were from Thermo: KLHDC2 (s24149) and DCAF16 (s29651). These siRNAs were used at a final concentration of 20 nM (before compound addition) and transfections were done using Opti-MEM (Thermo 119058021) and Lipofectamine RNAiMAX (Thermo 13778150). The 'No siRNA' samples were prepared by using water instead of siRNA in the transfection reactions. To measure BRD proteins, HiBiT-BRD4 cells were seeded in Opti-MEM (Thermo 11058021) supplemented with 5% FBS and were transfected the next day with siRNA using Lipofectamine RNAiMAX (Thermo 13778150) in Opti-MEM. After 2 d of siRNA treatment, compounds in DMSO were diluted in Opti-MEM supplemented with 5% FBS and then added to cells, with an overall dilution ratio of 1:400. After 4 h, cells were processed for immunoblots, and HiBiT signals were analyzed as described above. For AR, VCaP cells were seeded in DMEM without phenol red, supplemented with 10% FBS, and immediately treated with the siRNA-transfection mixtures. After 2 d, the medium was changed to the same DMEM base medium but this was supplemented with 5% charcoal-stripped FBS. Compounds were added to cells for 12 h (in the same medium), and 24 h after the medium change, and samples were processed for immunoblots. *KLHDC2*-targeting siRNAs used in the paper are listed in the table below (underlined nucleotides represent DNA).

Target Gene	Supplier	Catalog no.	Figure(s)	Sequence
<i>KLHDC2</i>	Thermo	S24149	Fig. 3f–j	GAUCUACAACAUGGAGACUGG
<i>KLHDC2</i>	OriGene	SR308385-A	Extended Data Fig. 4	CAGUAAAAUGAAUGGAUACAAU <u>T</u>
<i>KLHDC2</i>	OriGene	SR308385-B	Extended Data Figs. 2 and 4	GGAGGAUUUACCACUGAUAAACA <u>G</u> C
<i>KLHDC2</i>	OriGene	SR308385-C	Extended Data Fig. 4	GUAACAUCACAGAGUGGCAUCA <u>T</u>

In *KLHDC2* immunoblots, a band present in the cell extracts that migrated as an approximately 46-kDa species was not responsive to *KLHDC2*-targeting siRNA, despite knockdown of >90% *KLHDC2* mRNA being achieved (as measured by qPCR, see below and Extended Data Figure 2f) and large increases in the model nanoluc-based *KLHDC2* substrate under the same siRNA conditions (Extended Data Figs. 2 and 4). Therefore, this band is not *KLHDC2*, and endogenous *KLHDC2* was not detectable under the conditions we tested. Overexpression of *KLHDC2* led to emergence of a slightly faster migrating band in cell extracts, proving that the *KLHDC2* antibody can detect *KLHDC2* in cell extracts if enough *KLHDC2* is present.

qPCR was used to measure relative *KLHDC2* mRNA levels in HiBiT-BRD4 cells following treatment with si*KLHDC2* (OriGene, SR308385-B) or universal scrambled siRNA (OriGene), both in triplicate. RNA was isolated from cells using the RNeasy kit (Qiagen, 74004) and quantified using a NanoDrop microscale spectrophotometer. RNA was converted to cDNA using the High-Capacity cDNA Reverse Transcription Kit (Thermo 4368814). Control reactions lacking reverse transcriptase were included for each sample. qPCR was carried out using SsoAdvanced Universal SYBR Green Supermix (Bio-Rad) and a CFX96 Touch Real-Time PCR detection System (Bio-Rad). Primers for *KLHDC2* (Hs.PT.58.14583229) and *HPRT1* (Hs.PT.58v.45621572), the housekeeping gene, were from Integrated DNA Technologies. No signals were detected using cDNA synthesis samples that lacked reverse transcriptase. The  $2^{-\Delta\Delta CT}$  method was used to quantify fold-change differences between conditions. qPCR data are shown in tabular form in Extended Data Figure 2e.

### Screening the arrayed siRNA library

A Silencer Human Ubiquitin siRNA library in 96-well plate format was purchased from Thermo Fisher Scientific (A30141), and we generally followed the accompanying protocol for library screening with reverse transfection. Using an Agilent BRAVO, the siRNAs were resuspended in ultrapure water, and an aliquot of each was diluted in Opti-MEM, mixed with Opti-MEM and Lipofectamine RNAiMAX, and then aliquoted into wells of white-clear 96-well cell-culture plates. PC-3\_HiBiT-BRD4 cells that had been growing in large flasks were detached using trypsin and EDTA, diluted in Opti-MEM supplemented with 7% FBS, and were then seeded into the 96-well plates (which already contained the siRNA-transfection mixes) using a Multidrop Combi dispenser, for a final density of 20,000 cells per well. siRNAs were at a final concentration of 16 nM in the 96-well assay plates, before the compound was added. Column 12 of each plate contained controls: rows A–D had no siRNA (with water in its place) and rows E–H had *PSMD7*-targeting siRNA (Thermo, s11403). We also seeded two control plates, which had the column 12 controls but each included 16 wells (columns 1 and 2) that would receive no degrader in the subsequent step. After 3 d of incubation, Opti-MEM supplemented with 5% FBS containing compound 1 was added to all wells of each 96-well plate, except for those in columns 1 and 2 of the two control plates. Compound 1 was used at a final concentration of 50 nM, achieved through a 1:400 overall dilution from DMSO stocks. After 2 h of treating cells with compound 1 (plates were staggered), assay plates were processed using the Nano-Glo HiBiT Lytic Detection System, as described above. We calculated mean luminescence for the 32 ‘no degrader’ wells on the two control plates and then used this value to calculate ‘percent no degrader’ for all other wells. The 4 ‘no siRNA’ wells of each plate, 268 in total across all plates,

had a mean of 7.4% with a s.d. of 0.7%. We used a cutoff of >9.5%, which is  $7.4\% + 3 \times \text{s.d.}$ , to determine that a well was a hit. Then, for each gene, a ‘hit score’ was determined, which refers to how many wells for a given gene were called hits. Certain siRNAs that were ineffective at blocking the degrader may have been ineffective at knocking down the protein, but the likelihood that a gene is important for degradation increases with hit score.

### High-mass MALDI mass spectrometry

For high-mass, intact MALDI analysis, measurements were taken using an Autoflex II MALDI ToF mass spectrometer (Bruker) equipped with CovalX’s HM4 interaction module. The following parameters were used. Mass spectrometer: linear and positive mode; ion source 1: 20 kV; ion source 2: 17 kV; lens: 12 kV; pulse ion extraction: 400 ns; HM4: gain voltage: 3.14 kV; acceleration voltage: 20 kV. For analysis, 20  $\mu\text{L}$  of each protein sample (KBC and KBC–SelK peptide) were pipetted to prepare eight dilutions with final volume of 10  $\mu\text{L}$ . These eight dilutions of the samples were prepared to obtain concentrations ranging from 1 mg  $\text{mL}^{-1}$ –8  $\mu\text{g mL}^{-1}$ . For control reactions, 1  $\mu\text{L}$  of each dilution was mixed with 1  $\mu\text{L}$  of a matrix composed of a re-crystallized sinapinic acid matrix (10 mg  $\text{mL}^{-1}$ ) in acetonitrile/water (1:1, vol/vol), TFA 0.1% (K200 MALDI Kit). After mixing, 1  $\mu\text{L}$  of each sample was spotted on the MALDI plate (SCOUT 384). After crystallization at room temperature, the plate was placed in the MALDI mass spectrometer and analyzed immediately in high-mass MALDI mode. The analysis was repeated in triplicate. The cross-linking experiments allow direct analysis of non-covalent interactions by high-mass MALDI MS. By mixing a protein sample in which there are non-covalent interactions with a specially developed cross-linking mixture<sup>51</sup>, it is possible to specifically detect non-covalent complexes with high sensitivity. The covalent binding allows the interacting species to survive the sample-preparation process and the MALDI ionization. Using a special high-mass detection system, the interaction to be characterized in the high-mass range. Each mixture prepared for the control experiment (9  $\mu\text{L}$  remaining) was subjected to cross-linking using CovalX’s K200 MALDI MS analysis kit. Nine microliters of the mixtures (ranging from undiluted to 1/128) were mixed with 1  $\mu\text{L}$  of K200 stabilizer reagent (2 mg  $\text{mL}^{-1}$ ) and incubated at room temperature. After incubation for 180 min, the samples were prepared for MALDI analysis, as was done for control experiments. The samples were analyzed by high-mass MALDI immediately after crystallization.

### Analytical size-exclusion chromatography

All reaction mixtures were incubated for 1 h at 25 °C before analysis. Concentrations listed in the figures were prepared in 50  $\mu\text{L}$  reactions. Running buffer contained 50 mM Hepes pH 7.5, 50 mM NaCl, and 1 mM TCEP. Samples for Figure 4a,e were run on a Superose 6 5/150 column; samples for Figure 5e and Extended Data Figure 7b were run on a Superdex 200 5/150 column. Experiments were repeated at least twice, and representative gels are shown.

### Cryo-EM sample preparation and data collection and processing

KBC was buffer exchanged into 50 mM Hepes pH 7.5, 150 mM NaCl, and 1 mM TCEP, and diluted to 18  $\mu\text{M}$ . Bis(sulfosuccinimidyl)suberate (BS3; Thermo Scientific Pierce) was prepared to 25 mM according to the manufacturer’s instructions. BS3 was added to a final concentration

of 900  $\mu\text{M}$  to KBC, and the mixture was incubated for 1 h at 15 °C. The reaction was quenched with 1 M Tris and run on a Superdex 200 5/150 column pre-equilibrated with reaction buffer. Pure fractions were collected and concentrated to 5 mg ml<sup>-1</sup>.

Cryo-EM grids were frozen on Quantifoil Active grids on a chameleon grid-freezing robot (SPT Labtech) in single-stripe mode with a plunge time of 206 ms after a 20-s online glow discharge at 12 mA. Data were collected on two grids, one with a protein concentration of 18  $\mu\text{M}$  and one with a protein concentration of 9  $\mu\text{M}$ . Preliminary analysis demonstrated that there was a diversity of particle orientations. A Titan Krios G3i operating at 300 keV equipped with a Gatan Quantum Life Science energy filter and a K3 direct electron detection camera was used to collect data. Videos were collected, as summarized in Table 1. A total of 10,382 videos were collected and processed.

Movies were imported into cryoSPARC 3.3.1 (ref. 52) and processed using patch-based motion correction and contrast transfer function correction. Videos were further examined and 8,409 exposures were selected for further processing. Circular blobs were used to pick particles on 250 micrographs, which were further extracted and submitted to 2D classification. Templates were selected and used to pick particles on all micrographs. Selected particles were extracted at 2 $\times$  binning. After two rounds of 2D classification and selection of classes, the resulting 1,639,885 particles were re-extracted at full resolution with a box size of 320 pixels. Particles were submitted to ab initio reconstruction with six classes, and one class demonstrated good density for four KLHDC2 kelch domains. A homogeneous refinement was performed on this class to obtain alignments, and then the particles were subjected to a 3D variability analysis<sup>26</sup> in cryoSPARC4.1.1. The results were assessed in cluster mode with 20 clusters, and it became obvious that the heterogeneity in the data set resulted from different subunits of EloB–EloC not being present (Extended Data Fig. 6). Particles from five clusters were combined and subjected to non-uniform refinement<sup>27</sup>, local resolution estimation, and local filtering. The unsharpened map was used for model building owing to the high *B* factors associated with the novel parts of the map. Rigid-body docking of the crystal structure of the AlphaFold model of KLHDC2 and EloB–EloC from PDB 5T35 were performed in Phenix<sup>53</sup> with dock\_in\_map. The structure was refined with rounds of model building in coot and real-space refinement with Phenix. Figures were generated in ChimeraX.

### Reporting summary

Further information on research design is available in the Nature Portfolio Reporting Summary linked to this article.

### Data availability

Data are available and coordinates have been deposited at the PDB under accession numbers PDB 8SGE (KLHDC2<sub>KD</sub>–KDRLKZ-1), PDB 8SGF (KLHDC2<sub>KD</sub>–peptide C terminus), and PDB 8SH2 (apo-KBC) for the crystal structures. Cryo-EM maps for KLHDC2 have also been deposited at the Electron Microscopy Data Bank under accession numbers EMD-40477 (apo-KBC). In addition, the following published crystallographic data sets were used in this study: PDB 6DO3; PDB 5T35. Source data are provided with this paper.

### References

- Cardote, T. A. F., Gadd, M. S. & Ciulli, A. Crystal structure of the Cul2–Rbx1–EloBC–VHL ubiquitin ligase complex. *Structure* **25**, 901–911 (2017).
- Buckley, D. L. et al. Targeting the von Hippel–Lindau E3 Ubiquitin Ligase Using Small Molecules To Disrupt the VHL/HIF-1 $\alpha$  Interaction. *J. Am. Chem. Soc.* **134**, 4465–4468 (2012).
- Schrödinger Release 2023-1: Maestro (Schrödinger, 2021).
- Sastry, G. M., Adzhigirey, M., Day, T., Annabhimoju, R. & Sherman, W. Protein and ligand preparation: parameters, protocols, and influence on virtual screening enrichments. *J. Comput. Aided Mol. Des.* **27**, 221–234 (2013).
- Bowers, K. J. et al. Scalable algorithms for molecular dynamics simulations on commodity clusters. in *SC '06: Proc. of the 2006 ACM/IEEE Conference on Supercomputing* 43 (IEEE, 2006)
- Vonrhein, C. et al. Data processing and analysis with the autoPROC toolbox. *Acta Crystallogr. D Biol. Crystallogr.* **67**, 293–302 (2010).
- McCoy, A. J. et al. Phaser crystallographic software. *J. Appl. Crystallogr.* **40**, 658–674 (2007).
- Emsley, P., Lohkamp, B., Scott, W. G. & Cowtan, K. Features and development of Coot. *Acta Crystallogr. D Biol. Crystallogr.* **66**, 486–501 (2010).
- Emsley, P. & Cowtan, K. Coot: model-building tools for molecular graphics. *Acta Crystallogr. D Biol. Crystallogr.* **60**, 2126–2132 (2004).
- Bich, C. et al. Reactivity and applications of new amine reactive cross-linkers for mass spectrometric detection of protein–protein complexes. *Anal. Chem.* **82**, 172–179 (2010).
- Punjani, A., Rubinstein, J. L., Fleet, D. J. & Brubaker, M. A. cryoSPARC: algorithms for rapid unsupervised cryo-EM structure determination. *Nat. Methods* **14**, 290–296 (2017).
- Liebschner, D. et al. Macromolecular structure determination using X-rays, neutrons and electrons: recent developments in Phenix. *Acta Crystallogr. D Biol. Crystallogr.* **75**, 861–877 (2019).

### Acknowledgements

We thank I. Taylor for helpful comments on the manuscript; I. Drulyte, Y. Xiong, and A. Fathizadeh for helpful tips and discussions on cryo-EM data processing; and C.-j. Lee and H. Huang for assistance with crystallography data.

### Author contributions

Data collection and analysis—C.M.H., K.M.D., A.H., K.Z., D.R.L., A. Chapman, A.P., C.Q., P.G., B.T., J.D., J.C., M.B.; manuscript preparation—C.M.H., K.M.D., A.H., K.Z., D.R.L., A.M.C., M.B. (writing, reviewing, figure preparation). All authors have read and commented on the manuscript. Corresponding author: M.B.

### Competing interests

All authors are, or have been, employees and shareholders of Arvinas Inc, which is developing PROTAC molecules for therapeutic applications.

### Additional information

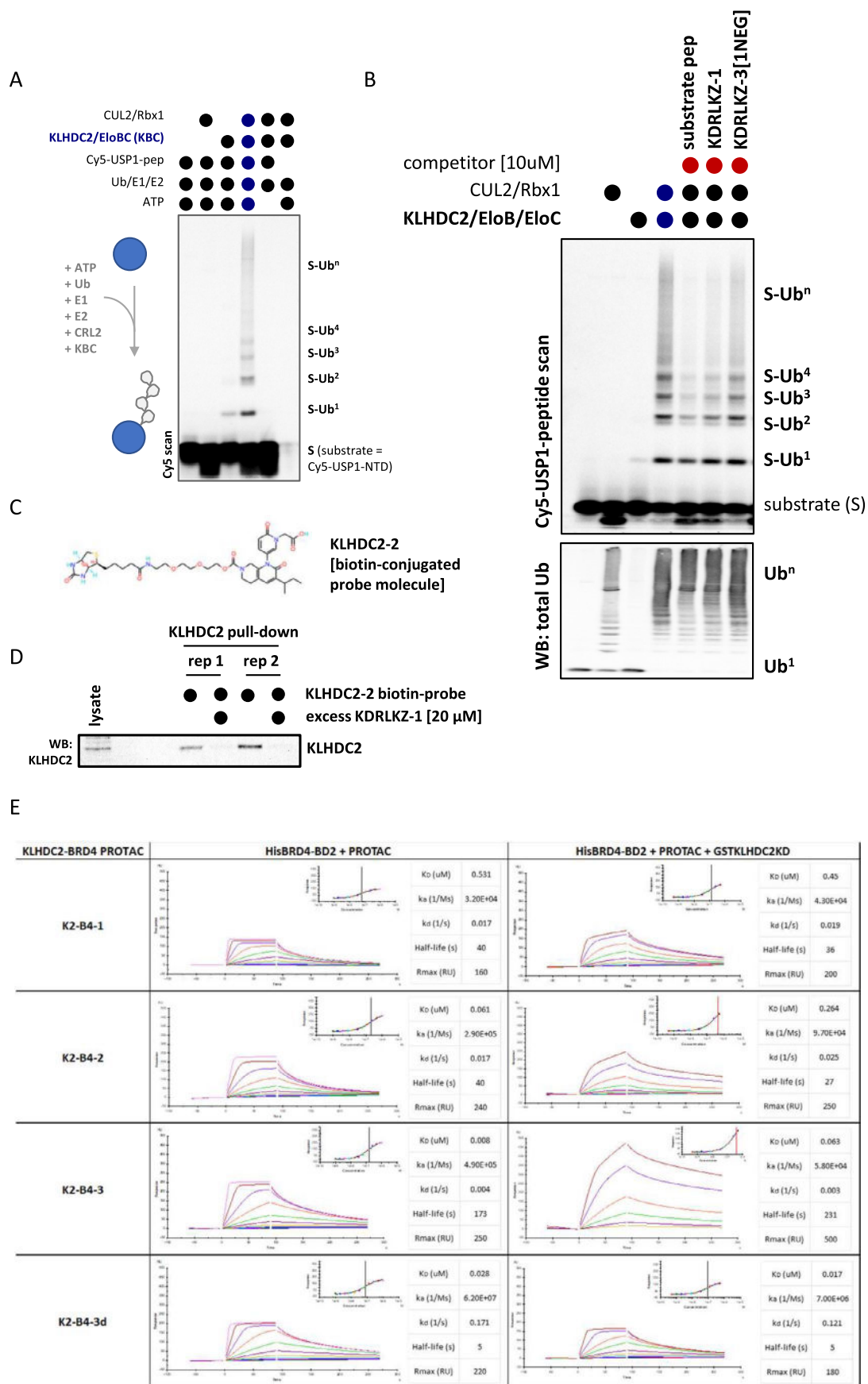
**Extended data** is available for this paper at <https://doi.org/10.1038/s41594-023-01146-w>.

**Supplementary information** The online version contains supplementary material available at <https://doi.org/10.1038/s41594-023-01146-w>.

**Correspondence and requests for materials** should be addressed to Miklós Békés.

**Peer review information** *Nature Structural & Molecular Biology* thanks the anonymous reviewers for their contribution to the peer review of this work. Dimitris Typas was the primary editor on this article and managed its editorial process and peer review in collaboration with the rest of the editorial team.

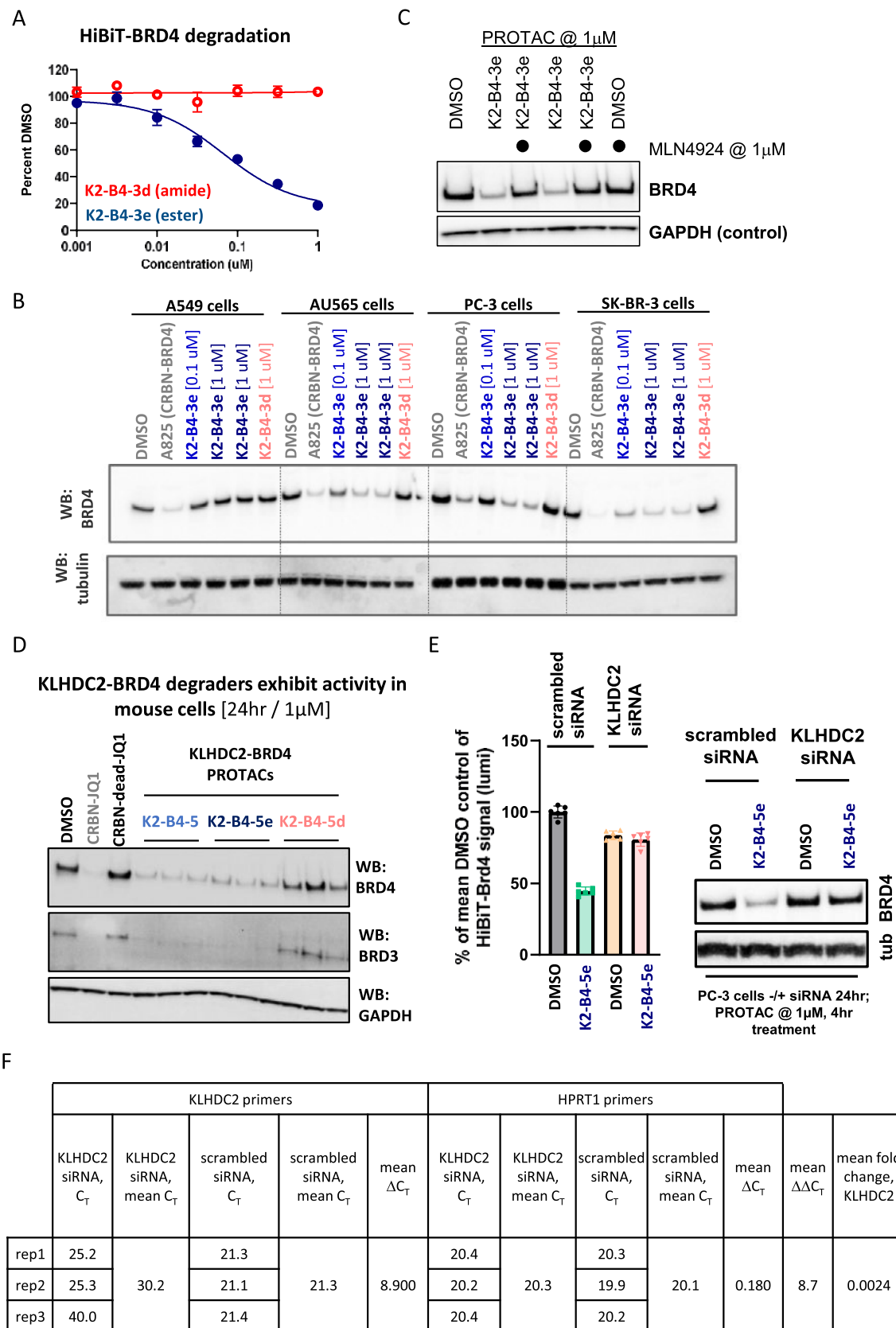
**Reprints and permissions information** is available at [www.nature.com/reprints](http://www.nature.com/reprints).



Extended Data Fig. 1 | See next page for caption.

**Extended Data Fig. 1 | Additional biochemical characterization of KLHDC2 ligands.** **a)** In vitro ubiquitylation reactions of a Cy5-conjugated USP1 C-terminal peptides by KLHDC2/EloB/EloC (representative gel shown of two independent experiments). **b)** In vitro ubiquitylation reactions of a Cy5-conjugated USP1 C-terminal peptides in the presence and absence of KLHDC2-targeting small molecules (representative gel shown of two independent experiments).

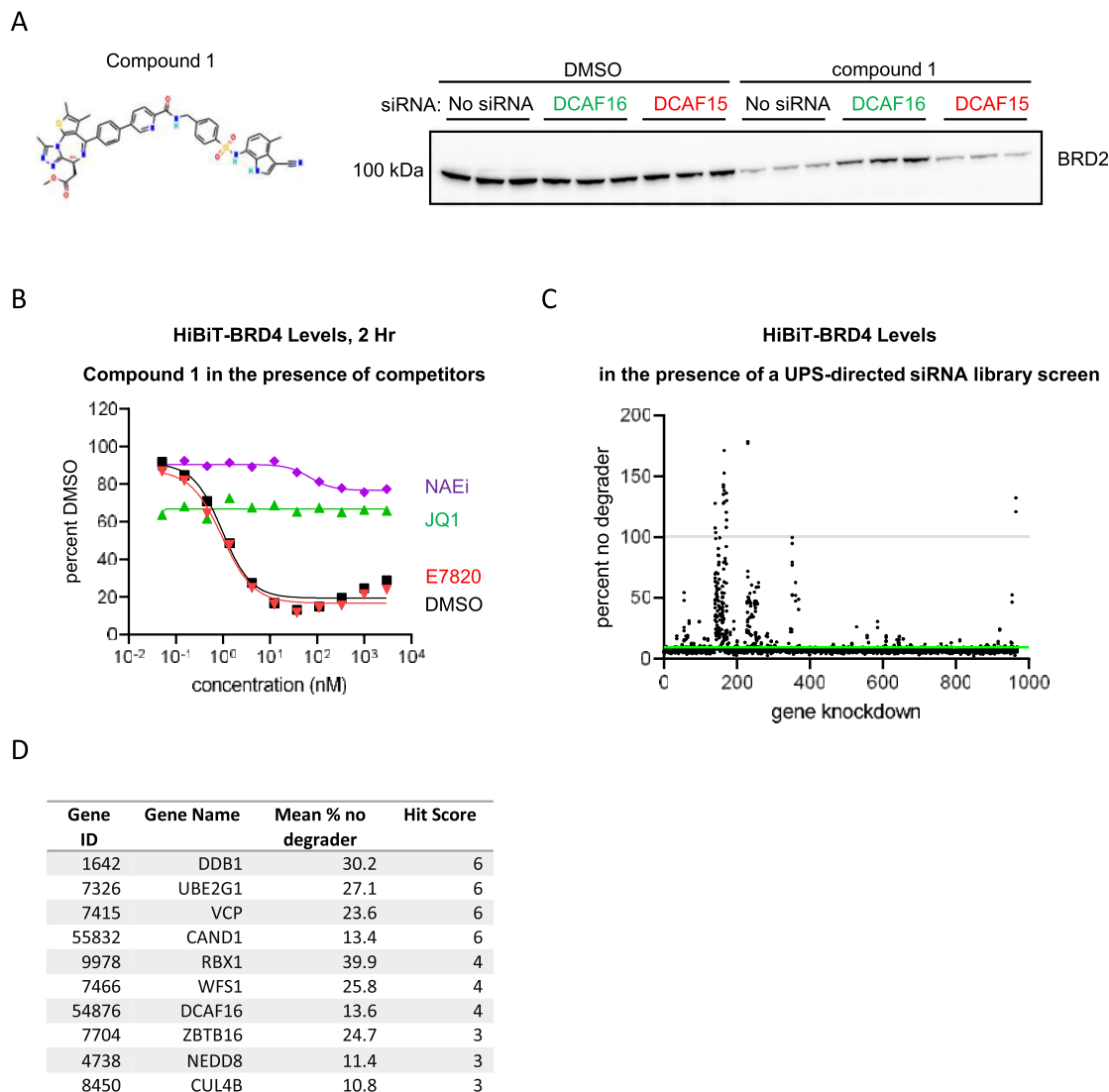
**c)** Structure of a biotin-conjugated KLHDC2 ligand used in Fig. 2a,b. **d)** KLHDC2 pull-down using probe above in C) in the absence and presence of competing excess KDRLKZ-1, analyzed by anti-KLHDC2 immunoblot, performed in duplicate. **e)** Ternary complex SPR sensograms and kinetic values (related to Figs. 2d and e), K2-B4-3 sensograms are duplicated in this Extended Data panel for completion).



Extended Data Fig. 2 | See next page for caption.

**Extended Data Fig. 2 | Additional cell-based characterization of KLHDC2-based degraders.** **a)** HiBiT-BRD4 levels were measured following 24 hr treatment of PC-3\_HiBiT-BRD4 cells with the indicated PROTACs (n = 4 replicates). **b)** Endogenous BRD4 levels were measured across cell lines by immunoblots following 24 hr treatment with the K2-B4-3e PROTAC, and its controls (dotted lines included for clarity, one of two independent gels shown). **c)** Endogenous BRD4 levels were measured by immunoblot following 24 hr treatment of PC-3 cells with the K2-B4-3e PROTAC, with and without co-treatment with 1 mM MLN4924. **d)** Endogenous BRD4 and BRD3 levels were measured by immunoblots

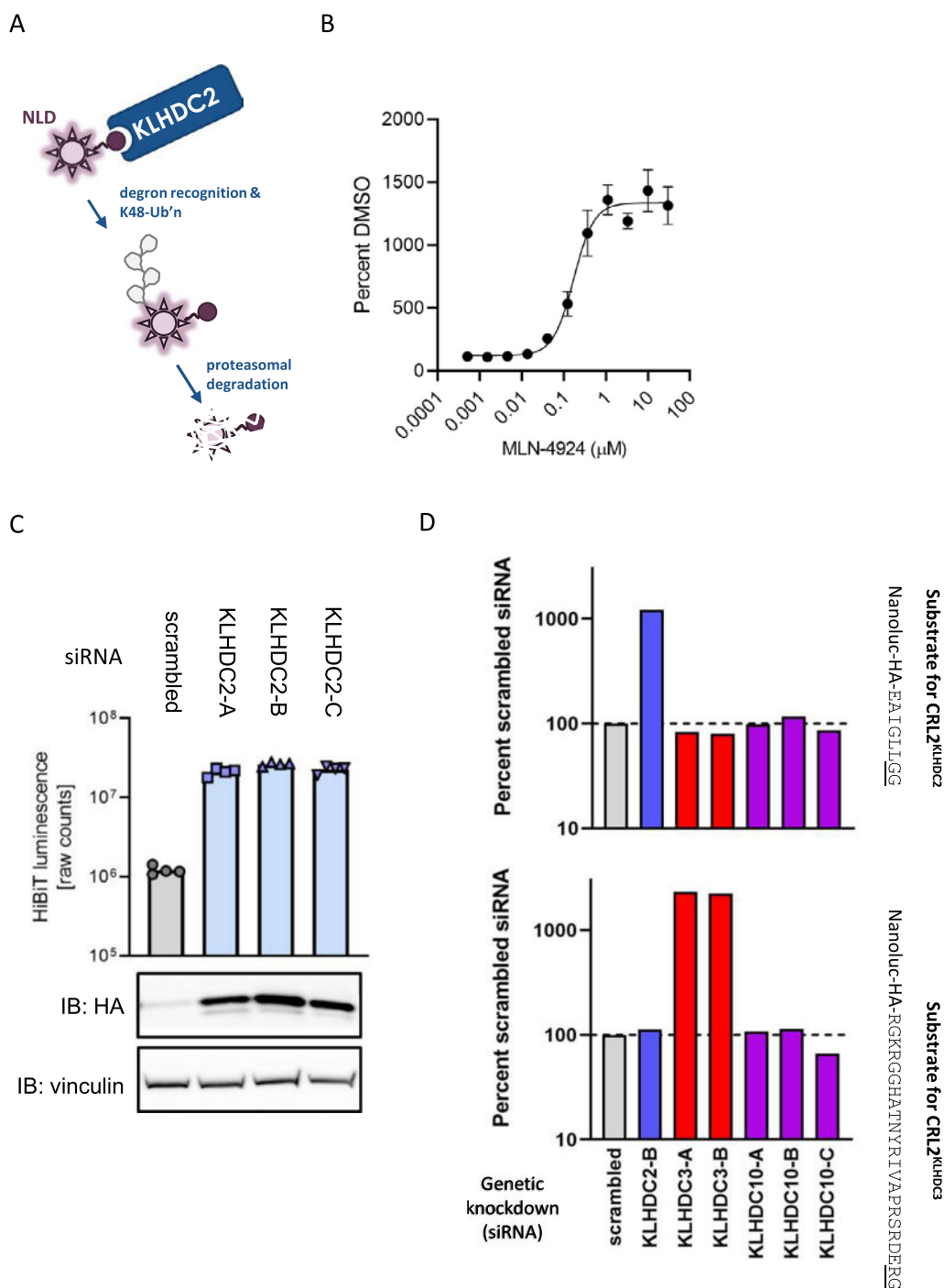
following 24 hr treatment of mouse A20 cells by the indicated PROTACs at 1  $\mu$ M (n = 3 technical replicates). **e)** Left panel, HiBiT-BRD4 levels were measured from cells treated with the indicated siRNAs for 48 hours, then treated with the K2-B4-5e PROTAC for 4 hr (n = 2 biological replicates with n = 3 technical replicates); and right panel, anti-BRD4 immunoblot data from the same experiment (representative of triplicate blots). **f)** In a parallel set of wells, relative mRNA levels were measured by qPCR after siRNA treatment of cells, in triplicate (see Methods).



### Extended Data Fig. 3 | UPS-wide siRNA screen against compound 1.

**a)** Structure of compound 1 (left) and (right) PC-3\_HiBiT-BRD4 cells were treated in triplicate for a total of 72 hours with siRNA to the indicated gene (or no siRNA as a control) with either DMSO or 50 nM compound 1 (in triplicate) added for the final 2 hours before collecting samples for immunoblots for BRD2. **b)** PC-3\_HiBiT-BRD4 cells were treated with the indicated potential inhibitors of compound 1 action 30 min prior to treatment with the indicated concentrations of compound 1 for 2 hours. NAEi was used at 1  $\mu$ M while JQ1 and E7820 were used at 10  $\mu$ M. The 'DMSO' curve in this part shows mean  $\pm$  SD data based on duplicate measures per dose whereas the other curves are based on singlicate measures per dose. **c)** PC-3\_HiBiT-BRD4 cells were screened with a siRNA library covering 968 genes, listed on the x-axis. Percent of the mean for the 'no degrader wells' (from a total of 32 wells on two control plates) is graphed for the 6 individual data points per gene

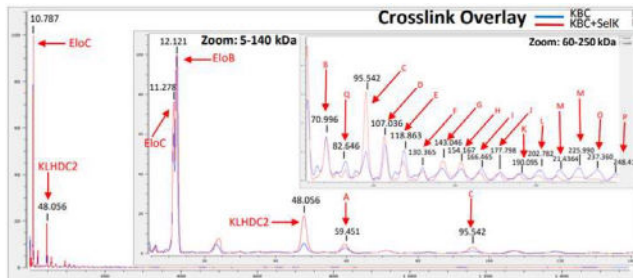
(from 6 wells, duplicates for 3 separate siRNAs per gene). The green horizontal line shows the threshold used for calling hits, based on mean + 3-fold SD of the 'no siRNA' condition across plates. The cluster showing many points with relatively high values for gene #s 140-175 are all genes for proteasome subunits. The genes for ubiquitin, also common hits in the screen, are at positions 228-230 on the graph. **d)** Table showing siRNA screen data for genes with a hit score of 3 out of 6 or greater, not including genes for ubiquitin or the proteasome. The 'no siRNA' wells in the screen (n = 268, 4 per 96-well plate) had a mean of 7.4% with a SD of 0.7%. We used a cutoff of >9.5%, which is 7.4% + 3xSD, to call a well a hit. Hit score refers to how many wells for a given gene were called hits. 'Mean % no degrader' in this table includes all 6 values for the gene, even those wells which were not hits.



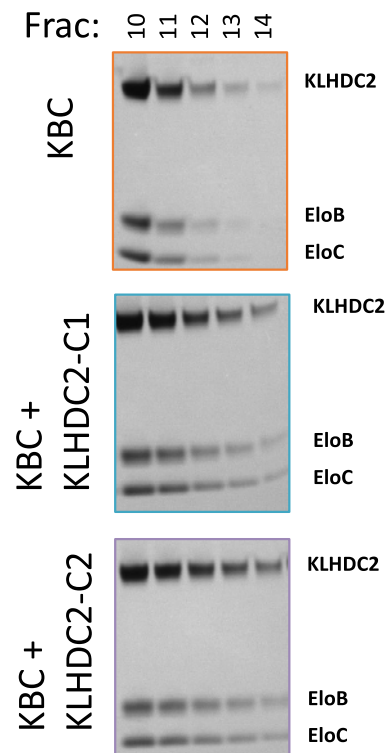
**Extended Data Fig. 4 | Characterization of the NLD (NanoLuc-degron) system for KLHDC2.** **a)** Cartoon representation of the NLD assay. **b)** MLN4924 dose-response curve showing the stabilization of a CRL2KLHDC2-degron in the NLD assay using the Nano-Glo detection system ( $n = 2$  replicates shown). **c)** CRL2KLHDC2-degron NLD signal is stabilized with KLHDC2 siRNA treatments

shown by a Nano-Glo readout ( $n = 3$  replicates), as well as anti-HA immunoblot for the stabilized protein. **d)** Nano-Glo readout of a CRL2KLHDC2-degron and a CRL2KLHDC3-degron stability by KLHDC2, KLHDC3 and KLHDC10 siRNAs – showing specific stabilization by the respective degrons for KLHDC2 and KLHDC3. Error bars represent mean + SD.

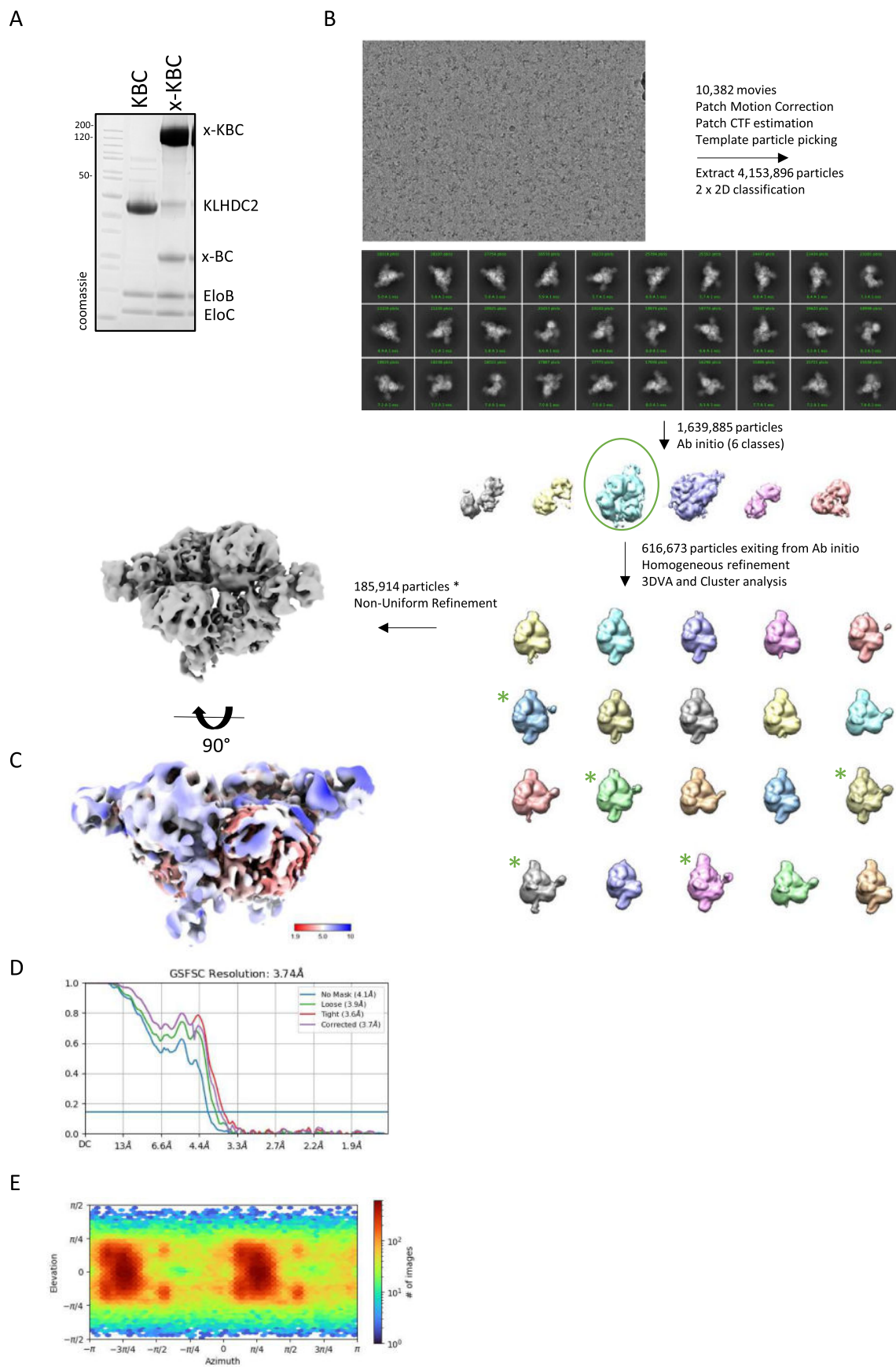
A



B



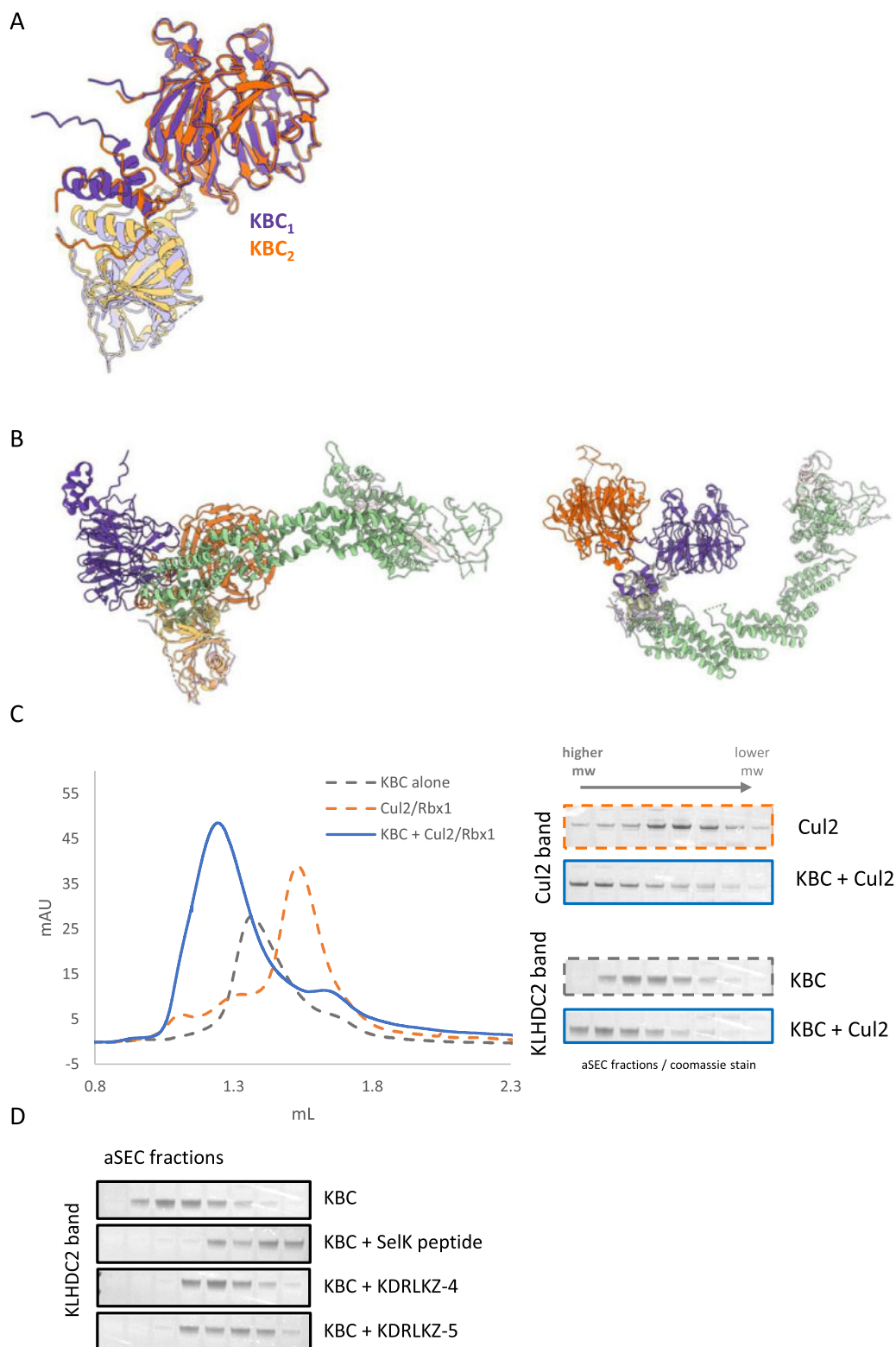
**Extended Data Fig. 5 | Additional characterization of KBC complexes by MALDI and aSEC. a)** Peaks in the high mass MALDI experiment show that KLHDC2/EloB/EloC is a higher-order oligomer that dissociates into smaller subcomplexes upon binding substrate. **b)** SDS-PAGE gels of KBC complexes incubated with peptides shown in Fig. 4e, stained with Coomassie.



Extended Data Fig. 6 | See next page for caption.

**Extended Data Fig. 6 | Cryo-EM processing workflow of the KLHDC2-EloB-EloC tetramer.** **a)** SDS-PAGE analysis of cross-linked KBC complexes in preparation for cryoEM. **b)** Overview of processing workflow, from raw micrographs to final map shown in Fig. 5a. Upon ab initio calculation, multiple

3D classes were obtained that demonstrate dimeric, trimeric, and tetrameric assemblies of KBC. Further analysis was focused on the tetrameric assembly. All steps performed in cryoSPARC 3.3.1 and 4.1.1. **c)** Local resolution mapped onto final map. **d)** FSC plot. **e)** Viewing distribution for the final reconstruction.



**Extended Data Fig. 7 | Characterization of KBC complexes by CUL2 binding and compounds.** **a**) Overlay of the structure models of the two non-identical KBC units within the tetramer. **b**) EloC from PDB ID 5n4w aligned to model in paper. Orange KLHDC2 is not competent for binding Cul2 (left). Purple KLHDC2 is competent for binding Cul2 (right). **c**) Size Exclusion chromatograms demonstrating elution profiles of 10  $\mu$ M KBC (grey), 10  $\mu$ M Cul2/Rbx1 (orange),

and a mixture of 10  $\mu$ M KBC and 10  $\mu$ M Cul2/Rbx1 (blue). The elution of the mixture to earlier elution volumes demonstrates interaction of KBC and Cul2/Rbx1, which can also be seen in the SDS-PAGE gel of the fractions collected (stained with Coomassie). **d**) SDS-PAGE gels of KBC complexes incubated with small molecules shown in Fig. 5f.

## Reporting Summary

Nature Portfolio wishes to improve the reproducibility of the work that we publish. This form provides structure for consistency and transparency in reporting. For further information on Nature Portfolio policies, see our [Editorial Policies](#) and the [Editorial Policy Checklist](#).

### Statistics

For all statistical analyses, confirm that the following items are present in the figure legend, table legend, main text, or Methods section.

- | n/a                                 | Confirmed  |
|-------------------------------------|--|
| <input type="checkbox"/>            | <input checked="" type="checkbox"/> The exact sample size ( $n$ ) for each experimental group/condition, given as a discrete number and unit of measurement  |
| <input type="checkbox"/>            | <input checked="" type="checkbox"/> A statement on whether measurements were taken from distinct samples or whether the same sample was measured repeatedly  |
| <input checked="" type="checkbox"/> | <input type="checkbox"/> The statistical test(s) used AND whether they are one- or two-sided<br><i>Only common tests should be described solely by name; describe more complex techniques in the Methods section.</i>  |
| <input checked="" type="checkbox"/> | <input type="checkbox"/> A description of all covariates tested  |
| <input checked="" type="checkbox"/> | <input type="checkbox"/> A description of any assumptions or corrections, such as tests of normality and adjustment for multiple comparisons   |
| <input type="checkbox"/>            | <input checked="" type="checkbox"/> A full description of the statistical parameters including central tendency (e.g. means) or other basic estimates (e.g. regression coefficient) AND variation (e.g. standard deviation) or associated estimates of uncertainty (e.g. confidence intervals) |
| <input checked="" type="checkbox"/> | <input type="checkbox"/> For null hypothesis testing, the test statistic (e.g. $F$ , $t$ , $r$ ) with confidence intervals, effect sizes, degrees of freedom and $P$ value noted<br><i>Give <math>P</math> values as exact values whenever suitable.</i>                                       |
| <input checked="" type="checkbox"/> | <input type="checkbox"/> For Bayesian analysis, information on the choice of priors and Markov chain Monte Carlo settings  |
| <input checked="" type="checkbox"/> | <input type="checkbox"/> For hierarchical and complex designs, identification of the appropriate level for tests and full reporting of outcomes  |
| <input checked="" type="checkbox"/> | <input type="checkbox"/> Estimates of effect sizes (e.g. Cohen's $d$ , Pearson's $r$ ), indicating how they were calculated  |

*Our web collection on [statistics for biologists](#) contains articles on many of the points above.*

### Software and code

Policy information about [availability of computer code](#)

- |                 |   |
|-----------------|---|
| Data collection | CryoEM data was collected on a Titan Krios G3i microscope, operating at 300keV equipped, with a Gatan Quantum Life Science energy filter and K3 direct electron detection camera. X-ray diffraction data was collected on a Advanced Photon Source IMCA-CAT beamline. Intact mass data was collected on a Autoflex II MALDI ToF mass spectrometer (Bruker) equipped with CovalX's HM4 interaction module. SPR data was collected on Biocore 8K+ (binary data) and Biacore S200 (ternary data), Cytvia. (See methods for details.)   |
| Data analysis   | De novo ligand design was performed in Schrodinger Maestro using the Protein Preparation Wizard (). Graphs were prepared using GraphPad PRISM (v9.4.1). SPR data was analyzed and graphed by Biacore Insight Evaluation Software (). X-ray dataset were integrated and scaled with autoPROC and PHASER, refined by BUSTER and models built in COOT . CryoEM movies were prepared by cryoSPARC, and 3D variability analysis was performed using cryoSPARC v4.1.1, Phenix was used for rigid body fitting. Images were prepared by Pymol v2.0 and ChimeraX v1.4. (See methods for details.) |

For manuscripts utilizing custom algorithms or software that are central to the research but not yet described in published literature, software must be made available to editors and reviewers. We strongly encourage code deposition in a community repository (e.g. GitHub). See the Nature Portfolio [guidelines for submitting code & software](#) for further information.

## Data

Policy information about [availability of data](#)

All manuscripts must include a [data availability statement](#). This statement should provide the following information, where applicable:

- Accession codes, unique identifiers, or web links for publicly available datasets
- A description of any restrictions on data availability
- For clinical datasets or third party data, please ensure that the statement adheres to our [policy](#)

Coordinates have been deposited at the Protein Data Bank (PDB) under accession numbers PDB 8SGE (KLHDC2KD:KDRLKZ-1), PDB 8SGF (KLHDC2KD:C-term-pep), and PDB 8sh2 (KBC-apo). Cryo-EM maps have been deposited at the Electron Microscopy Data Bank (EMDB) under accession numbers EMD-40477 (KBC apo). In addition, the following datasets were used in this study: PDB 6DO3; PDB 5T35. PDB validation reports are provided as supplementary material.

## Research involving human participants, their data, or biological material

Policy information about studies with [human participants or human data](#). See also policy information about [sex, gender \(identity/presentation\), and sexual orientation](#) and [race, ethnicity and racism](#).

Reporting on sex and gender	<input type="text" value="Does not apply."/>
Reporting on race, ethnicity, or other socially relevant groupings	<input type="text" value="Does not apply."/>
Population characteristics	<input type="text" value="Does not apply."/>
Recruitment	<input type="text" value="Does not apply."/>
Ethics oversight	<input type="text" value="Does not apply."/>

Note that full information on the approval of the study protocol must also be provided in the manuscript.

## Field-specific reporting

Please select the one below that is the best fit for your research. If you are not sure, read the appropriate sections before making your selection.

Life sciences       Behavioural & social sciences       Ecological, evolutionary & environmental sciences

For a reference copy of the document with all sections, see [nature.com/documents/nr-reporting-summary-flat.pdf](https://www.nature.com/documents/nr-reporting-summary-flat.pdf)

## Life sciences study design

All studies must disclose on these points even when the disclosure is negative.

Sample size	<input type="text" value="n=2 biological replicate minimum (listed in Figure legends)"/>
Data exclusions	<input type="text" value="no data was excluded"/>
Replication	<input type="text" value="data represents a minimum of two biological replicates (where applicable - see Methods and Figure legends for details)."/>
Randomization	<input type="text" value="We did not rely on experiments where randomization was necessary (ie no animal studies conducted)."/>
Blinding	<input type="text" value="We did not rely on experiments where blinding was necessary (ie no animal studies conducted)."/>

## Reporting for specific materials, systems and methods

We require information from authors about some types of materials, experimental systems and methods used in many studies. Here, indicate whether each material, system or method listed is relevant to your study. If you are not sure if a list item applies to your research, read the appropriate section before selecting a response.

## Materials &amp; experimental systems

n/a	Involvement in the study
<input type="checkbox"/>	<input checked="" type="checkbox"/> Antibodies
<input type="checkbox"/>	<input checked="" type="checkbox"/> Eukaryotic cell lines
<input checked="" type="checkbox"/>	<input type="checkbox"/> Palaeontology and archaeology
<input checked="" type="checkbox"/>	<input type="checkbox"/> Animals and other organisms
<input checked="" type="checkbox"/>	<input type="checkbox"/> Clinical data
<input checked="" type="checkbox"/>	<input type="checkbox"/> Dual use research of concern
<input checked="" type="checkbox"/>	<input type="checkbox"/> Plants

## Methods

n/a	Involvement in the study
<input checked="" type="checkbox"/>	<input type="checkbox"/> ChIP-seq
<input checked="" type="checkbox"/>	<input type="checkbox"/> Flow cytometry
<input checked="" type="checkbox"/>	<input type="checkbox"/> MRI-based neuroimaging

## Antibodies

Antibodies used	anti-KLHDC2 @ 1:1000 (Thermo, PA5-90252), anti-ubiquitin @ 1:5000 (CST, #3933), anti-BRD2 @ 1:1000 (CST, #5848), anti-BRD4 @ 1:1000 (abcam, ab243862), anti-tubulin @ 1:5000 (CST, #6074)
Validation	Literature validated antibodies had been used, except the KLHDC2 antibody which recognized recombinant KLHDC2 and pull-down-enriched KLHDC2 from lysates, as well as over-expressed KLHDC2

## Eukaryotic cell lines

Policy information about [cell lines and Sex and Gender in Research](#)

Cell line source(s)	Cell lines were purchased from ATCC (cell line suppliers listed in the methods). PC3 parental, PC3-HiBit-BRD4 (CS3023130), A549, AU565, SK-BR-3, and Sf21 (insect cells) for protein expression.
Authentication	Cell lines were purchased from ATCC and maintained according manufacturer's protocol, routinely checked for mycoplasma contamination (Lonza Mycoplasma detection kit MycoAlertPlus #LT07-710), but were not further authenticated.
Mycoplasma contamination	All cell lines tested negative for mycoplasma contamination (by Lonza Mycoplasma detection kit MycoAlertPlus #LT07-710)
Commonly misidentified lines (See <a href="#">ICLAC</a> register)	None